

# Integrating brain and biomechanical models - a new paradigm for understanding neuro-muscular control

**Sebastian James**<sup>1,2</sup>, **Chris Papapavlou**<sup>5</sup>, **Alexander Blenkinsop**<sup>1,2</sup>,  
**Alexander Cope**<sup>3</sup>,

**Sean Anderson**<sup>2,4</sup>, **Konstantinos Moustakas**<sup>5</sup>, **Kevin Gurney**<sup>1,2,\*</sup>

<sup>1</sup> *Adaptive Behaviour Research Group, Department of Psychology, The University of Sheffield, Sheffield, UK*

<sup>2</sup> *Insigneo Institute for in-silico Medicine, The University of Sheffield, Sheffield, UK*

<sup>3</sup> *Department of Computer Science, The University of Sheffield, Sheffield, UK*

<sup>4</sup> *Department of Automatic Control Systems Engineering, The University of Sheffield, Sheffield, UK*

<sup>5</sup> *Department of Electrical and Computer Engineering, The University of Patras, Patras, Greece*

Correspondence\*:

Kevin Gurney

Department of Psychology, The University of Sheffield, Western Bank, Sheffield, S10 2TP, UK, k.gurney@sheffield.ac.uk

## 2 ABSTRACT

To date, realistic models of how the central nervous system governs behaviour have been restricted in scope to the brain, brainstem or spinal column, as if these existed as disembodied organs. Further, the model is often exercised in relation to an *in vivo* physiological experiment with input comprising an impulse, a periodic signal or constant activation, and output as a pattern of neural activity in one or more neural populations. Any link to behaviour is inferred only indirectly via these activity patterns. We argue that to discover the principles of operation of neural systems, it is necessary to express their behaviour in terms of physical movements of a realistic motor system, and to supply inputs that mimic sensory experience. To do this with confidence, we must connect our brain models to neuro-muscular models and provide relevant visual and proprioceptive feedback signals, thereby closing the loop of the simulation. This paper describes an effort to develop just such an integrated brain and biomechanical system using a number of pre-existing models. It describes a model of the saccadic oculomotor system incorporating a neuromuscular model of the eye and its six extraocular muscles. The position of the eye determines how illumination of a retinotopic input population projects information about the location of a saccade target into the system. A pre-existing saccadic burst generator model was incorporated into the system, which generated motoneuron activity patterns suitable for driving the biomechanical eye. The model was demonstrated to make accurate saccades to a target luminance under a set of environmental constraints. Challenges encountered in the development of this model showed the importance of this integrated modelling approach. Thus, we exposed shortcomings in individual model components which were only apparent when these

were supplied with the more plausible inputs available in a closed loop design. Consequently we were able to suggest missing functionality which the system would require to reproduce more realistic behaviour. The construction of such closed-loop animal models constitutes a new paradigm of *computational neurobehaviour* and promises a more thoroughgoing approach to our understanding of the brain's function as a controller for movement and behaviour.

Keywords: integrated brain biomechanics neuromuscular oculomotor saccade basal ganglia

## 1 INTRODUCTION

Note: Changes based on Reviewer 1's comments are in this colour. For Reviewer 2 we use this colour.

The field of computational neuroscience has provided many *systems models* of the brain (Arai et al., 1994; Gancarz and Grossberg, 1998; Hazy et al., 2007; Blenkinsop et al., 2017). We refer to these as *mechanistic computational models*, meaning models which consist of populations of neural elements, interconnected in a biologically plausible manner, which simulate the operation of the brain. Whilst they differ in scale and complexity, these models all seek to describe the fundamental mechanisms behind common animal behaviours such as locomotion, threat evasion, reaching or feeding. However, none of the models cited here actually reproduce these behaviours. In each case, the activity in a certain population of neurons is taken to be representative of a behavioural outcome. In some cases, it is reasonable to take the activity of an internal population within the brain model as being representative of the induced behaviour. For example, a choice made in a *go/no-go* task could be determined from activity in a population within a basal ganglia model (Nambu et al., 1990; Khn et al., 2004). The decision to *go* is selected by a reduction of activity in this population; maintenance of activity implies *no-go*. To validate the model, the error rates which it generates could be compared with experimentally determined error rates in primate subjects. We refer to this as an *output assumption model* because the output is assumed to signify behaviour. (An *input assumption model* assumes that sensory input produces some particular form of neural activity in an input population of the model.)

However, we may be interested in reproducing accurate simulated *trajectories*, in order to find out how degradation of parts of the model affect movement. In Parkinson's Disease, degradation of the dopamine neurons originating in the substantia nigra pars compacta (SNc) causes diskinesia (Galvan and Wichmann, 2008), as well as abnormal network activity in the basal ganglia (Brown et al., 2001; McCarthy et al., 2011). Sufferers of the disease would be expected to produce abnormal decision-making and movement trajectories in a reach-to-the-correct-target task such as the one described in James et al. (2017). A model which sought to explore in detail the effects of the SNc degradation both on the decision making and on the movement dynamics would need a physically accurate virtual arm, as well as physically realistic sensory input for the brain. This is no less than a complete model of those sections of the brain and body which act to fulfil the task. Such a modelling effort, if successful, would result in a virtual robot capable of expressing behaviour in response to sensory input from its environment. This would represent a paradigm shift in the field of computational neuroscience worthy of the new name of *computational neurobehaviour*.

In an attempt to build a model combining brain, realistic biomechanics and sensory feedback, we sought to extend our previous work modelling the oculomotor system by adding a virtual, biomechanical eye model able to make physically realistic movements. The rotational state of the eye would then determine how visual features in the virtual world were projected back into the brain model. The existing model (Cope et al., 2017) is already able to capture sensory input and convert it into a neural signal, assumed to specify the target of a *saccadic eye movement*; a fast movement of the eyes which directs the fovea to

64 a region of interest in the field of view. The oculomotor system is an excellent candidate for modelling  
65 because its movements can be specified with only three degrees of freedom, making it one of the simplest  
66 neuro-muscular systems in the body. It is nevertheless behaviourally interesting, as saccadic eye movements  
67 reveal information about decision making at a subconscious level (Deubel and Schneider, 1996; Reppert  
68 et al., 2015; Marcos and Genovesio, 2016). The modelling of the oculomotor system is served by a large  
69 body of behavioural data describing saccades (Tipper et al., 2001; Walker et al., 1997; Casteau and Vitu,  
70 2012), many anatomical studies of the neural substrates involved (Meredith and Ramoa, 1998; Isa, 2002;  
71 Isa and Hall, 2009) and electrophysiological data linking these together (Hepp and Henn, 1983; Dorris et al.,  
72 1997; McPeek et al., 2003; Vokoun et al., 2011). Furthermore, in the context of building *behaving* systems,  
73 a necessary part of any model for which the behaviour requires visual attention and decision making is a  
74 realistic mechanism for gathering visual information. This is obvious from extrinsic considerations—a  
75 subject must look at a scene to make decisions or navigate within it. It also follows for *intrinsic* reasons.  
76 For example, Howard and Tipper (1997) showed that visual cues affect reach trajectories and the same  
77 group later demonstrated that reaching affects the saccadic system (Tipper et al., 2001) suggesting a close  
78 relationship between these neural systems. **Building a behaving oculomotor system will therefore assist**  
79 **future computational neurobehavioural modelling efforts that involve reaching.**

80 Many neural populations are involved in the coding of saccadic eye movements, only a very brief  
81 overview is given here; for a review, see Munoz (2002). One pathway takes information from the retina  
82 directly into the superficial layers of the superior colliculus in the brainstem (Sterling, 1971; Linden and  
83 Perry, 1983; Wu et al., 1994). Activity within the superior colliculus then excites neurons in the pons,  
84 medulla and rostral mid-brain (Sparks, 2002). and **finally the motor neurons** which innervate the extraocular  
85 muscles (Fuchs and Luschei, 1970; Sparks, 2002). This direct pathway is responsible for the low latency  
86 saccades called express saccades (Schiller et al., 1987; Edelman and Keller, 1996). Information from the  
87 retina is also processed by visual cortex which feeds through to the frontal eye fields in which activity is  
88 related to reflexive and voluntary saccades (Schall and Thompson, 1999). Activity build-up in the frontal  
89 eye fields is transferred to the intermediate layers of the superior colliculus (Stanton et al., 1988b) and is  
90 also processed by the basal ganglia, which participates in the selection of the winning saccade end point  
91 (Stanton et al., 1988a; Hikosaka et al., 2000). Although both cortical and subcortical paths produce a  
92 saccade target signal in the superior colliculus, it is also possible for animals to make relatively normal  
93 saccades even after the colliculus has been ablated (Wurtz and Goldberg, 1972; Aizawa and Wurtz, 1998),  
94 though express saccades are lost with collicular lesions (Schiller et al., 1987). This makes the superior  
95 colliculus a perplexing structure, being both critically involved in saccade target specification (Sparks and  
96 Nelson, 1987) and saccade dynamic control (Waitzman et al., 1991; Goossens and van Opstal, 2012) and  
97 yet dispensible. The ‘backup pathway’ likely incorporates the oculomotor vermis and fastigial oculomotor  
98 region of the cerebellum which are known to participate in the specification, dynamics and adaptation of  
99 saccadic eye movements (Kleine, 2003; Takagi et al., 1998).

100 There is a long history of modelling the oculomotor system. For a comprehensive review, see Girard and  
101 Berthoz (2005). Models of individual **sub-systems** have been proposed for brainstem (Robinson, 1975;  
102 Scudder, 1988; Gancarz and Grossberg, 1998), cerebellum (Quaia et al., 1999; Dean, 1995; Dean et al.,  
103 1994) and superior colliculus (Arai et al., 1994; Morn et al., 2013; Marino et al., 2012). More recently,  
104 combined models have also been developed incorporating sensory input (Cope et al., 2017) and driving **a**  
105 **second order differential equation** representing the eye (Tabareau et al., 2007; N’Guyen et al., 2014; Thurat  
106 et al., 2015). None of these models has yet fully closed the loop to produce a behaving system operating  
107 freely within its environment. We argue that developing integrated, closed-loop models of behaving systems

108 offers insights into the operation of neural systems that are not available from input- or output-assumption  
109 models.

## 2 MATERIAL & METHODS

110 The integrated brain and biomechanical model described here is a development of the model in Cope  
111 et al. (2017), referred to here as the Cope-Chambers-Prescott-Gurney model. This was a rate-coded neural  
112 network model incorporating retinal populations, frontal eye fields (FEF), the basal ganglia (BG), and  
113 the superior colliculus (SC). The Cope-Chambers-Prescott-Gurney model takes as *input* the positions  
114 of luminances (of fixed shape and intensity) on a topographic map. Whilst certain assumptions were  
115 made about the input—that a luminant input excites activity on a retinotopic layer, with computer code  
116 carrying out the transformation achieved in the brain by a neural connectivity map (Thivierge and Marcus,  
117 2007)—it is nonetheless *not* an input-assumption model according to our definition because the activity  
118 generated in the neural input layer is modelled as a response to the luminances, rather than being crafted.  
119 In the Cope-Chambers-Prescott-Gurney model, the centroid of the activity in the deep layers of superior  
120 colliculus was assumed to accurately encode the location of the eye at the end of the saccade (Wurtz and  
121 Goldberg, 1972; Robinson, 1972; Van Gisbergen et al., 1987; McIlwain, 1982). This location was used to  
122 recalculate the positions of the luminances in the eye’s frame of reference at each time step. Because a  
123 pattern of neural activity in the output population was assumed to have a behavioural outcome, it was thus  
124 an *output-assumption model*. The model included no brainstem populations other than superior colliculus,  
125 nor a neuromuscular model.

126 To the Cope-Chambers-Prescott-Gurney model, we added a brainstem model and a biomechanical eye  
127 model. The rate-coded brainstem model was taken from the literature (Gancarz and Grossberg, 1998)  
128 as the best-of-breed saccadic burst generator (Girard and Berthoz, 2005). The biomechanical eye was  
129 implemented using the biomechanical modelling framework OpenSim; the brain and brainstem were  
130 modelled using the SpineML toolchain. These will be described below, along with a review of the  
131 Cope-Chambers-Prescott-Gurney model, but first we will give a description of the co-ordinate systems.

### 132 2.1 Co-ordinates in the world

133 Before describing the biomechanical eye and the brain model, which consisted of retinotopically mapped  
134 neural sheets, we describe the co-ordinate system used in the world. The eye was located at the origin of a  
135 three-dimensional, right-handed Cartesian co-ordinate system, with its fovea directed in the  $-z$  direction.  
136 There was a notional spherical screen which was also centred at the origin of the co-ordinate system and  
137 had a radius of 50 (in arbitrary units). The *fixation point* was the point on the screen at which the eye  
138 was initially directed. Onto the screen were projected target luminances, each of which having a position  
139 described by two co-ordinates;  $\theta_x^t$ , a rotation of the horizon plane about the  $x$  axis, and  $\theta_y^t$ , a rotation of the  
140 meridian plane about the  $y$  axis. The position is the intersection of these rotated planes with the spherical  
141 screen (disregarding the intersection point of these three surfaces behind the eye). Note that a luminance  
142 with positive  $\theta_x^t$  was above the horizon of this world; one whose  $\theta_y^t$  was positive lay to the left of the  
143 world’s meridian. For this reason, many of the figures in this paper are plotted with  $-\theta_y$  on the  $x$ -axis and  
144  $\theta_x$  on the  $y$ -axis so that targets that lay up and to the right in the world do so in the graphs, also.

145 Luminances were crosses of height and width subtending  $\pm 3^\circ$  and whose ‘bars’ were  $2^\circ$  thick. Lumi-  
146 nances were oriented like + symbols with their vertical bar aligned with the meridian plane and their  
147 horizontal bar aligned with the horizon.

148 The eye's frame of reference was initially aligned with the world's frame of reference. At each timestep,  
149 the eye's rotational state (described by the Euler rotations  $\theta_x$ ,  $\theta_y$ ,  $\theta_z$ ) was used to translate the three  
150 dimensional Cartesian co-ordinates of the luminances in the world frame into co-ordinates in the eye frame.  
151 The luminance co-ordinates in the eye's frame of reference were used to determine the input to the brain  
152 model.

## 153 2.2 Existing brain model

154 The brain model, excluding the brainstem, is a re-implementation of the Cope-Chambers-Prescott-  
155 Gurney model, of reflexive saccadic behaviour (Cope et al., 2017). Reflexive saccades are fast eye  
156 movements elicited by abrupt changes in the peripheral visual scene (reflexive saccades can occur also as a  
157 result of auditory and somatosensory stimuli, but these modalities are ignored in this model). A reflexive  
158 saccade has a starting position defined by the initial orientation of the eye and an end-point position in  
159 which the eye is directed towards a new target. Regardless of the number of targets within the visual scene,  
160 the brain must choose one location as the end-point, because the eyes can look only in one direction at a  
161 time. The functionality reproduced by the Cope-Chambers-Prescott-Gurney model is 'the selection of the  
162 best target end-point for a reflexive saccade'. A competition such as this between incompatible movements  
163 is often referred to as an *action selection* problem (Norman and Shallice, 1986; Maes, 1989; Redgrave  
164 et al., 1999).

165 One hypothesis for the rôle played by the basal ganglia (BG) is that the system performs *action selection*  
166 (Mink, 1996; Redgrave et al., 1999; Hikosaka et al., 2000). The Cope-Chambers-Prescott-Gurney model  
167 places the BG at the centre of the oculomotor system, following the known anatomy of the region (Hikosaka  
168 et al., 2000). The BG receives input indirectly from the superior colliculus, which has a retinotopic  
169 arrangement (Ottes et al., 1986). The BG receives excitatory inputs directly from retinotopic regions of the  
170 cortex including the frontal eye fields (FEF), supplementary eye fields (SEF), lateral intraparietal cortex  
171 (LIP) and dorsolateral prefrontal cortex. The dorsolateral prefrontal cortex, which participates in voluntary  
172 saccades (Funahashi et al., 1993; Munoz and Everling, 2004), is not modelled because the model concerns  
173 reflexive rather than voluntary eye movements. Several other regions of the brain that are associated with  
174 eye movements are also omitted from the model. The early visual processing stream in cortex, from V1,  
175 through to the LIP is subsumed into a 'sustained retinal' signal which arrives at FEF. The justification here  
176 is that the model reacts to simple luminant targets and does not need to carry out the feature extraction  
177 performed by these visual areas. The supplementary eye fields are involved in the programming of saccade  
178 sequences (Tehovnik et al., 2000) and memory guided saccades (Chen and Wise, 1995; Schlag, 2002).  
179 Lesions of SEF do not affect visually guided saccades (Gaymard et al., 1998) and so the SEF is also omitted  
180 from the model.

181 Fig. 6(a) shows the macroscopic architecture of the Cope-Chambers-Prescott-Gurney model. The figure  
182 shows the relationships between the retinal input populations, the FEF, the populations comprising the BG  
183 sub-system (the red border indicates that the box represents a number of populations as a sub-system), the  
184 thalamus and the superior colliculus. Excitatory connections are indicated with arrow heads; inhibitory  
185 connections with circles in place of the arrow heads. The blue and green connection lines indicate two  
186 thalamo-basal ganglia loops, one cortical loop through FEF (green), the other a sub-cortical loop through  
187 SC. It is important to note that although they are given different colours in the diagram, these loops are in  
188 no way independent, with loop activity combining both in thalamus and in the basal ganglia and a direct  
189 excitatory, feed-forward connection from FEF to SC.

190 The basal ganglia sub-system is the most complex component of the Cope-Chambers-Prescott-  
191 Gurney model. The BG model is based on previous work (Gurney et al., 2001b,a) and is referred to  
192 as the GPR model. The GPR model incorporates the following main components of the primate BG  
193 (Mink, 1996; Wickens, 1997): (i) The striatum (the main input station to the BG) which is divided into two  
194 iterdigitated populations of projection neurons expressing primarily D1 or D2-type dopaminergic receptors  
195 (named Str\_D1 and Str\_D2); (ii) The subthalamic nucleus (STN); (iii) the external segment of the globus  
196 pallidus (GPe); (iv) the output nucleus relevant for saccadic control—the substantia nigra pars reticulata  
197 (SNr) (Hikosaka et al., 2000).

198 The connectivity of the GPR model [Fig. 6(b)] is constrained by the known anatomy and physiology of  
199 the BG (Bolam et al., 2000). Physiologically, the only source of glutamate within the BG is the STN, whose  
200 projections are therefore excitatory; all other nuclei have GABAergic projection neurons and are therefore  
201 inhibitory. The cortex sends glutamatergic projections to both the Str\_D1 striatal population, which projects  
202 preferentially to the SNr, and to Str\_D2, which projects primarily to GPe (Gerfen et al., 1990). The cortex  
203 also projects to the STN, which sends diffuse projections to the SNr and GPe (Parent and Hazrati, 1993).  
204 The GPe projects to the SNr and also projects back to the STN, completing a GPe–STN loop.

205 The GPR model is arranged into ‘action channels’; Fig. 6(b) shows an example network containing three  
206 channels. It is between these channels that competition occurs, with the winning channel succeeding in  
207 reducing activity in the output nucleus, SNr, and thereby disinhibiting its target. The complete connectivity  
208 pattern for this small network is shown in Fig. 6(b); the left channel in cortex innervates the left channels  
209 of Str\_D1, STN and Str\_D2. Connections are one-to-one, so it follows that the middle channel of cortex  
210 innervates the middle channels of STN and the striatal populations and the right channel of cortex innervates  
211 right channels in striatum and STN. Striatal population channels also inhibit SNr and GPe on a one-to-one  
212 basis and GPe feeds inhibition to SNr and STN in a one-to-one manner. The outputs from STN however  
213 are not one-to-one. The output from all channels of STN is summed together and then the sum is fed into  
214 each channel of SNr and GPe. This models the diffuse excitation from STN which has been observed in  
215 the BG (Parent and Hazrati, 1993).

216 Within the BG, there are several mechanisms supporting competitive processing for selecting channels  
217 whose inhibitory output should be reduced. The selection mechanism of the GPR model is the ‘off-centre,  
218 on-surround’ scheme proposed by Mink and Thach (1993). The ‘on-surround’ is provided by diffuse,  
219 excitatory projections from the STN to the SNr. Focussed inhibition from the Str\_D1 neurons in striatum  
220 contributes the ‘off-centre’ part of the mechanism. This arrangement leads to selection behaviour via a  
221 release of target inhibition, since channels that have strong salience (input) have weak output at the level of  
222 SNr, and channels with weak salience have enhanced output.

223 The GPe is not included in the centre-surround circuit described above, but still plays a key rôle in  
224 selection. Operating alone, the Str\_D1/STN/SNr circuit can suffer from the following problem: if the input  
225 for all channels is relatively high, then the diffuse projection from STN, which effectively supplies a sum  
226 of *all* of the STN inputs to each channel in SNr, will provide so much excitation that Str\_D1 may become  
227 unable to inhibit one of the channels in SNr and selection may become impossible. Gurney et al. (2001b,a)  
228 showed that the inhibitory feedback from GPe to STN acts as an ‘automatic gain control’ to help prevent  
229 this from occurring.

230 At the neuronal level, the STN, GPe and SNr have tonic output levels (Chevalier and Deniau, 1990;  
231 DeLong et al., 1985; Kita and Kitai, 1991). This is modelled using piecewise linear output functions  
232 with zero offsets,  $c$  (see Eq. 4) but with noise added to the input. In striatum, Str\_D1 and Str\_D2 have

positive offset  $c$ , mimicking the so-called ‘down-state’ of medium spiny neurons which have a resting potential far below spiking threshold and require co-ordinated input to generate action potentials (Wilson and Kawaguchi, 1996). In addition, the Str\_D1 and Str\_D2 neurons are influenced by dopamine in different ways; facilitating cortico-striatal transmission at medium spiny neurons with D1 receptors (Hernández-López et al., 1997; Gonon, 1997) and reducing transmission at those with D2 receptors (Delgado et al., 1999). These effects are modelled using a dopamine parameter which modulates the input activation as described below in Eqs 8 & 9; Str\_D1 activation is enhanced; Str\_D2 activation is suppressed.

The GPR model in Fig. ??(b) has only three channels with focussed inhibition from striatum to SNr and GPe defined by a simple one-to-one scheme. The action channels represent discrete, incompatible motor action choices. In the oculomotor model, an action channel might represent the end-point of saccade, and the competition carried out in the basal ganglia is between potential saccade end-points. However, eye movements have a *continuous* end-point space; the eye can rotate to any orientation within its biomechanically permissible range. Some end-points within this range are certainly mutually exclusive—it’s not possible to look to the left and to the right simultaneously—but *nearby* end-points are not necessarily incompatible. A small enough error in the end-point of a saccade will not prevent the eye from foveating on a target as the fovea is not infinitesimally small. To cope with this requirement, the populations within the oculomotor basal ganglia are conceived of as two-dimensional topographic grids of neural elements. Activity in each element corresponds to a spatial location in the visual field. ? here.

Add description of FEF. (FIXME).

Fig. 7 shows the layout of the populations in the brain model, as implemented in SpineCreator, and the interconnections between them. [Describe this figure in more detail. \(FIXME\)](#).

## 2.2.1 Components

With the exceptions of the World and FEF\_add\_noise populations, each neural element represents an activation; the activation is governed by a first order differential equation specified in the SpineML component. In the brain model, there are six different components in use: LINlinear; LINret; LINexp; D1MSN and D2MSN.

The LINlinear component governs the activation  $a$  with a first order leaky integrator differential equation:

$$\dot{a} = \frac{1}{\tau}(a_{in} - a) \quad (1)$$

where  $\tau$  is the time constant for the neural activation and  $a_{in}$  is the input to the neural element.  $a_{in}$  is defined by an activation input and a shunting inhibition input according to:

$$a_{in} = A(1 - s_a) + \alpha R_N \quad (2)$$

Here,  $A$  is the activation input and  $s_a$  is the shunting inhibition state variable whose value is related to the shunting input,  $S$  by

$$s_a = \begin{cases} S & S \leq 1 \\ 1 & S > 1 \end{cases} \quad (3)$$

$R_N$  is a random number drawn from a standard normal distribution ( $\sigma=1$ ,  $\mu=0$ ) and introduces noise to the activation of the neural element, with the parameter  $\alpha$  controlling the noise amplitude.

266 The output,  $y$ , of LINlinear is related to the activation  $a$  by the piecewise linear transfer function

$$y(a) = \begin{cases} 0 & a < c \\ a - c & c \leq a \leq 1 + c \\ 1 & a > 1 + c \end{cases} \quad (4)$$

267 where  $c$  is a parameter defining the offset of the transfer function. If  $c < 0$ , then for zero activation ( $a = 0$ ),  
 268 the output will be positive. This simulates the effect of a neural population having tonic firing. If  $c > 0$   
 269 then the output will be zero until the activation exceeds  $c$ , simulating neurons which only fire when driven  
 270 by excitatory input. At this point, the naming scheme for the component becomes apparent; this is a Leaky  
 271 Integrator with a piecewise-linear transfer function.

272 The LINret component used for the retinal populations is similar to the LINlinear component, but with  
 273 no intrinsic noise and no shunting inhibitory input. It has a neural input which is identical to the activation  
 274 input  $A$ :

$$a_{in} = A \quad (5)$$

275 The LINexp component is a leaky integrator with an exponential transfer function. It shares the same  
 276 differential equation with LINlinear, but has a different input equation and a different output transfer  
 277 function. It has the following equation for the neural element input  $a_{in}$ :

$$a_{in} = [A + N(a - V_r^-)](1 - S) + 0.01R_N \quad (6)$$

278 where  $A$  is the activation input and  $N$  is an input which is modulated by  $V_r^-$ , a reversal potential, and  
 279  $a$ , the current activation of the element. These inputs are summed and then reduced by a factor which  
 280 is dependent on  $S$ , the shunting input. As in LINlinear,  $R_N$  introduces normally distributed noise to the  
 281 element.

282 The output,  $y$ , of the LINexp component is given by

$$y(a) = \begin{cases} e^a - 0.9 & e^a \leq 1 + 0.9 \\ 1 & e^a > 1 + 0.9 \end{cases} \quad (7)$$

283 This component is used in the subthalamic nucleus (STN) population, as it gives a more physiologically  
 284 accurate f-I behaviour (Wilson, 2004; Bevan and Wilson, 1999; Hallworth et al., 2003) which has been  
 285 shown to allow the mapping of the basal ganglia network architecture onto an optimal decision making  
 286 model (Bogacz and Gurney, 2007).

287 The D1MSN and D2MSN components are both leaky integrators, similar to LINlinear. They differ in  
 288 that they have no shunting inhibition. They are used to model medium spiny neuron (MSN) populations  
 289 in the striatum. As they model the fact that most MSN neurons fall into two groups; those expressing D1  
 290 dopamine receptors and those expressing D2 receptors, they have a dopamine parameter that modulates the  
 291 input activation, so that their equations for  $a_{in}$  are thus:

$$a_{in}^{D1} = (0.2 + d)A + 0.01R_N \quad (8)$$

$$a_{in}^{D2} = (1 - d)A + 0.01R_N \quad (9)$$

293 where  $d$  is the dopamine parameter. Varying dopamine from 0 to 1 enhances the activation in the D1 model,  
 294 whereas it decreases the activation of the D2 model elements, in line with experimental observations  
 295 (Harsing and Zigmond, 1997; Gonon, 1997). Note that the equation for  $a_{in}^{D1}$  differs from that used in the  
 296 Cope-Chambers-Prescott-Gurney model, for which the cortico-striatal weights are multiplied by  $(1 + d)$   
 297 rather than  $(0.2 + d)$ .

298 The equations given above are applied to each element in a population. The value of the activation  $A$  (and  
 299 where relevant, the shunting input,  $S$ ) is determined by summing the weighted inputs to the population:

$$A = \sum_i w_i^{act} x_i^{act} \quad (10)$$

300

$$S = \sum_i w_i^{sh} x_i^{sh} \quad (11)$$

301  $w_i^{act}$  and  $w_i^{sh}$  are, respectively, the weights of the  $i^{th}$  activation or shunting connection;  $x_i^{act}$  and  $x_i^{sh}$  are  
 302 the signals input to the activation and shunting connections.

### 303 2.2.2 Population activity and retinotopic mapping

304 Each population of 2500 neural elements was arranged in a 50 by 50 grid, with positions on the grid  
 305 representing a retinotopic mapping similar to that found empirically both in the superior colliculus (Ottes  
 306 et al., 1986) and in visual cortex (Schwartz, 1980) and assumed in this work to persist throughout the  
 307 oculomotor system.

308 In a retinotopic mapping, the Cartesian co-ordinates of the light-sensitive cells in the retina, whose density  
 309 varies with distance from the fovea, are transformed into the Cartesian co-ordinates of the correspondingly  
 310 active cells on the colliculus. The mapping ensures that an even density of cells can be maintained in the  
 311 colliculus, but ensures that a group of adjoining, active, retinal neurons will always activate an adjoining  
 312 group of neurons on the collicular surface.

313 The mapping turns out to resemble polar co-ordinates. That is, one axis of the collicular surface specifies  
 314 the eccentricity of a retinal location (how far it is from the fovea) and the second axis specifies the rotational  
 315 angle of the retinal location; we therefore use the convention of referring to the eccentricity axis on the  
 316 colliculus as  $r$  and the rotation axis as  $\phi$ .

317 The *cortical magnification factor*,  $M(r)$ , gives the relationship between the radial eccentricity  $r$  and the  
 318 retinal neural density. As in Cope et al. (2017), we use a first-order approximation of the form for  $M(r)$   
 319 given in Rovamo and Virsu (1979):

$$M(r) = \frac{M_f}{1 + \frac{r}{E_2}} \quad (12)$$

320 The foveal magnification,  $M_f$ , is the magnification of the most central region of the retina and has a value  
 321 in the human of about 7.8 mm/ $^\circ$  (Rovamo and Virsu, 1979).

322 In our model,  $M_f$  is related to  $W_{nfs}$ , the width of the retinotopic neural field,  $W_{fov}$ , the width of the  
 323 eye's field of view and  $E_2$ , the eccentricity at which the retinal density has halved by:

$$M_f = \frac{W_{nfs}}{E_2 \ln \left( \frac{W_{fov}}{2E_2} + 1 \right)} \quad (13)$$

324 Here,  $W_{nfs}$  is 50 (the side length of the 50x50 grid) and  $W_{fov}$  is set to  $61^\circ$ , a reduction from the  
 325 biophysically accurate  $150^\circ$  due to the small number of neurons in the retinotopic neural field.  $E_2$  is 2.5  
 326 (Cope et al., 2017; Slotnick et al., 2001).

327 The mapping from the retinotopic co-ordinates in the brain to rotational co-ordinates of the stimulus/  
 328 response was written down by Schwartz (1977, 1980) for measurements of striate cortex [visual  
 329 stimulus to electrophysiological response—Daniel and Whitteridge (1961); Talbot and Marshall (1941)]  
 330 and by Ottes et al. (1986) for superior colliculus data [electrophysiological SC stimulus to eye movement  
 331 response—Robinson (1972)]. We used the following statement of this mapping to introduce stimuli into  
 332 the ‘World’ input population of the brain model:

$$\phi = \frac{W_{nfs}}{2\pi} \arctan \left( \frac{\theta_y^t}{\theta_x^t} \right) \quad (14)$$

333

$$r = M_f E_2 \ln \left( \frac{1}{E_2} \sqrt{\theta_x^{t^2} + \theta_y^{t^2}} + 1 \right) \quad (15)$$

344 Note that we use  $r$  and  $\phi$  as the co-ordinates on the ‘collicular surface’. Schwartz uses  $r$  and  $\phi$  as the polar  
 345 coordinates of the retinal stimulus; Ottes et al. use  $r$  and  $\phi$  as polar coordinates for the eye movement  
 346 response; both use  $u$  and  $v$  as the Cartesian co-ordinates of the neural map. We use  $\theta_x^t$  and  $\theta_y^t$  to give Euler  
 347 rotations for the retinal target stimulus. Note also that the form of Eqns. 14 & 15 is slightly different from  
 348 that given in Ottes et al. (1986) because our  $\theta_x^t$  and  $\theta_y^t$  are not the polar co-ordinates used in that work.

349 The mapping encompasses the entire visual field; the value of  $\phi$  is allowed to vary from  $0^\circ$  to  $360^\circ$  along  
 350 its axis. Effectively, the two contralateral colliculi found in the biology are incorporated into a single,  
 351 square map, avoiding the need to carry out the kind of ‘colliculus gluing’ described in Tabareau et al.  
 352 (2007).

343 It is straightforward to show that the reverse mapping is given by:

$$\theta_x = E_2 \left( e^{\frac{r}{M_f E_2}} - 1 \right) \cdot \cos \left( \frac{2\pi\phi}{W_{nfs}} \right) \quad (16)$$

344

$$\theta_y = E_2 \left( e^{\frac{r}{M_f E_2}} - 1 \right) \cdot \sin \left( \frac{2\pi\phi}{W_{nfs}} \right) \quad (17)$$

345 where we have dropped the  $t$  superscript on  $\theta_x$  &  $\theta_y$ , as these equations transform a collicular location into  
 346 rotations of the eye.

347 Fig. 8 shows the result of the mapping for a view of two cross-shaped luminances. One cross illuminates  
 348 the fovea, which results in a large comb-shape of activity. The more peripheral cross produces (in FEF) an  
 349 indistinct object centred at a larger value of  $r$ .

### 350 2.2.3 Network

351 Briefly, the model consists of input from the World population (see Fig. 7, green population box)  
 352 producing activity in an ‘express’ pathway to superior colliculus (purple) and simultaneously in cortex,  
 353 represented here by the FEF population (grey boxes in Fig. 7). The express pathway causes short latency  
 354 activity in the superficial superior colliculus, which directly innervates the deeper layers of the superior  
 355 colliculus (SC\_deep). Activity in FEF generates firing in a thalamo-cortico-basal ganglia loop. The output

356 of the basal ganglia is the substantia nigra pars reticulata (SNr) which tonically inhibits SC\_deep. If a  
357 location of activity in FEF is able to dominate selection in the basal ganglia circuit, the corresponding  
358 location in SNr will dis-inhibit and activity will build up in SC\_deep encoding the saccade end point.

359 Connections shown in red are one to one connections; dark blue projections indicate a connectivity pattern  
360 which ‘fans out’ with a 2-D Gaussian kernel; lighter blue connections from the subthalamic nucleus (STN)  
361 to SNr and globus pallidus externum (GPe) are diffuse, all-to-all connections and projections coloured  
362 green are one-to-one connections that decay towards the fovea so that foveal activity in FEF does not swamp  
363 the basal ganglia which would prevent peripheral luminances from ever being selected. Note that SC\_deep  
364 contains two recurrent connections; one is excitatory, with a Gaussian kernel mapping and the other  
365 implements tecto-tectal inhibition, which increases the inhibition between activity in opposite hemispheres  
366 of the field of view (Gian G. Mascetti and Jorge R. Arriagada, 1981; Olivier et al., 2000) helping to resolve  
367 competition between saccades to the left and right. The tecto-tectal inhibitory connection is *not* present in  
368 the Cope-Chambers-Prescott-Gurney model. In all other respects the model is as described in Cope et al.  
369 (2017). We have not listed the parameters of the network in tabular form here, instead, the reader is referred  
370 to the SpineML declarative specification of the model from the link given in SUPPLEMENTAL DATA.  
371 The easiest way to access this information is by using SpineCreator.

### 372 2.3 Brainstem model

373 We implemented a saccadic burst generator (SBG) based on the connectivity outlined in Gancarz and  
374 Grossberg (1998). The SBG network for two of the model’s six channels is shown in Fig. 9. We use the  
375 word ‘channel’ to mean a set of populations of neurons which are involved in actuating a single extraocular  
376 muscle. SBG channels are arranged in pairs, actuating opposing muscles. There is one pair of channels  
377 which actuates the superior and inferior rectus muscles, causing vertical rotations of the eye in a roughly  
378 parasaggital plane (the eye moves up or down). Another pair actuates the lateral and medial rectus muscles,  
379 causing horizontal rotations of the eye. The third pair actuates the superior and inferior oblique muscles  
380 which contribute to vertical as well as oblique rotations. Activity from the output layer of superior colliculus  
381 (SC\_avg) is fed into each channel, which sums the activity it receives and processes it in populations each of  
382 a single neural element representing all the neurons in that population. Each channel of the SBG functions  
383 to create the motor neuron activations that are required to accelerate the eye in a particular direction, then  
384 hold the eye in its new position against the returning force generated by the elastic properties of the muscles.  
385 The required motor neuron activations are therefore a combination of features: a brief burst of increased  
386 activity that accelerates the eye; followed by a period of activity that is less than the burst firing rate but  
387 higher than the tonic rate that exists when the eye is at the centre. This holds the eye in its new position.

388 The SBG connectivity produces each of the these features separately, then sums them to create the desired  
389 ‘bump and tonic’ activation time series. The input to the first population in the SBG, the long-lead burst  
390 neurons (LLBNs), is conceived as originating from one of the deep layers of the superior colliculus. The  
391 activity of the LLBNs are passed to excitatory burst neurons (EBNs) which, in turn, inhibit the LLBNs via  
392 the activity of the inhibitory burst neurons (IBNs). This feedback loop has a transmission delay, which  
393 allows activity to build up in the EBNs before the inhibition is activated and the activity is then reduced  
394 again. This mechanism generates the ‘bump’.

395 The generation of the ‘tonic’ phase of the required time series is achieved simply by integrating the bump  
396 over time and multiplying by a some small gain factor. This is the function of the tonic neurons (TNs).  
397 The firing rate of the motor neuron defines the amount of force applied to the eye by that muscle. Thus,  
398 the integral of the ‘bump’ defines how far the eye moves in that channel’s direction. The gain and delay

parameters in the LLBN-EBN-IBN-LLBN feedback loop therefore have to be tuned such that the endpoint of the saccade is reasonably accurate. Furthermore the restoring force generated by the elasticity of the muscles is dependent on the radial distance. The value of the new tonic firing rate, after the ‘bump’ is dependent on the end location of the eye. If the ratio between the EBN firing rate and the TN firing rate is not exactly correct, the eye will drift away from the saccade endpoint after the saccade has been completed. The EBN-TN connection strength is therefore tuned such that the TN firing rate yields a stable eye position across a range of eye eccentricities.

The omnipause neurons (OPNs) are tonically active and inhibit the EBNs. The activity of the OPNs is itself inhibited by activity in the LLBNs. The purpose of this arrangement is to ensure the eye does not move in response to neural noise.

Each mean activity of all the neurons in each SBG population (except the TNs) is defined by a single leaky integrator, first order differential equation.

$$\frac{da}{dt} = \frac{1}{\tau}(y - a) \quad (18)$$

where  $a$  is the activation of the nucleus, and  $\tau$  is the time constant of the nucleus.  $y$  is a piecewise linear function of the weighted sum of inputs to the nucleus and is given by

$$y(IN) = \begin{cases} 0 & IN \leq b \\ IN - b & b \leq IN \leq 1 + b \\ 1 & IN \geq 1 + b \end{cases} \quad (19)$$

where  $b$  is the  $IN$  axis offset.  $IN$  is the weighted sum of inputs to the nucleus and is given by,

$$IN = \sum_m^M w_{mn} a_m \quad (20)$$

where  $a_m$  is the activation of the  $m^{th}$  afferent nucleus.  $w_{mn}$  is the connection strength between the  $m^{th}$  afferent nucleus and the current nucleus. The activity of the TNs are defined as

$$\frac{da}{dt} = \frac{1}{\tau} y \quad (21)$$

with an identical piecewise linear transfer function as the other SBG populations.

## 2.4 Biomechanical eye

The output signals of the brainstem are used to drive the biomechanical model. The latter is not only used to get tangible feedback on the simulated saccades including motion trajectories, but adds one more modelling dimension related to the inertial properties of the eye plant including muscle properties.

The biomechanical eye model, implemented using the OpenSim framework (Seth et al., 2011), is anatomically represented by a sphere of uniform mass distribution. The diameter of the eye is 24 mm for adults, with small variations between individuals; the mass of the eye is 7.5 grams. The eyeball is actuated by six extraocular muscles (EOMs). The EOMs are arranged in three pairs forming a cone inside the orbit with the apex being located inside the cranium in a tendonous ring called the annulus of Zinn. An important

426 feature of the oculomotor system which greatly affects its overall behavior is the existence of dynamic  
 427 EOM pulleys. Their role is to guide the pivot point of the EOMs. In our model, a pulley for each EOM has  
 428 been modeled by a point on the orbit whose location depends on the current eye orientation.

429 An illustration of the biomechanical eye model is given in Figure 1, while Figure 2 depicts the head  
 430 model used in the proposed framework.

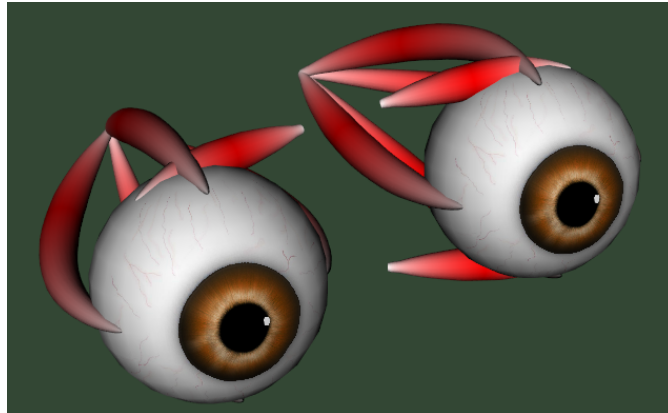


**Figure 1.** Example of the biomechanical eye model.

431 Two types of muscle models of different complexity are supported. The first models muscles using linear  
 432 path actuators. This simplistic model of ideal muscles can be easily integrated with high level brain models.  
 433 As described above the muscles are wrapped around the eye. The more complex model supported is based  
 434 on the Thelen model (Thelen, 2003) that is also supported by OpenSim and implements Hill-type muscles.  
 435 It includes realistic muscle wrapping geometric entities of the muscle fibers, while it accommodates for  
 436 both activation and contraction dynamics. The dynamics of muscular forces can be split into: 1) The  
 437 elasticity of the muscles. 2) A delay between the onset of the afferent excitatory signal and the actual  
 438 muscle contraction, caused by the transmission time of the action potentials and by the necessary calcium  
 439 release at the muscle fibres.

440 The force applied by EOMs is controlled by an excitatory signal supplied by motoneurons in the brainstem.  
 441 The neural drive to produce a saccadic eye movement can be characterized by a pulse component to  
 442 overcome the viscoelasticity of the orbital plant, a step component to stabilize the eye in the new position,  
 443 and a slide component that models the gradual transition between the pulse and step.

444 Passive forces due to the fatty tissues inside the eye orbit also affect eye dynamics. Their role is critical in  
 445 eliminating the influence of head and body movements. We incorporated a custom torque,  $t$ , which acts  
 446 like a rotational spring-damper apparatus, resisting eyeball movements. It has elastic and viscous properties  
 447 governed by  $t = -KR - CU$  where  $R$  is the eye's orientation and  $U$  is its angular velocity.  $K$  and  $C$  are  
 448 constants. A fuller description of the biomechanical model can be found in Papapavlou and Moustakas  
 449 (2014).

## 450 2.5 Model development framework

451 The Cope-Chambers-Prescott-Gurney model was originally developed to run on the BRAHMS model  
 452 execution framework (Mitchinson et al., 2010; Mitchinson and James, 2015). To run a BRAHMS model, the  
 453 researcher must develop *BRAHMS components* for the various neural elements. A BRAHMS component is  
 454 a programmatically coded implementation of the behaviour of the component. It may have an arbitrary

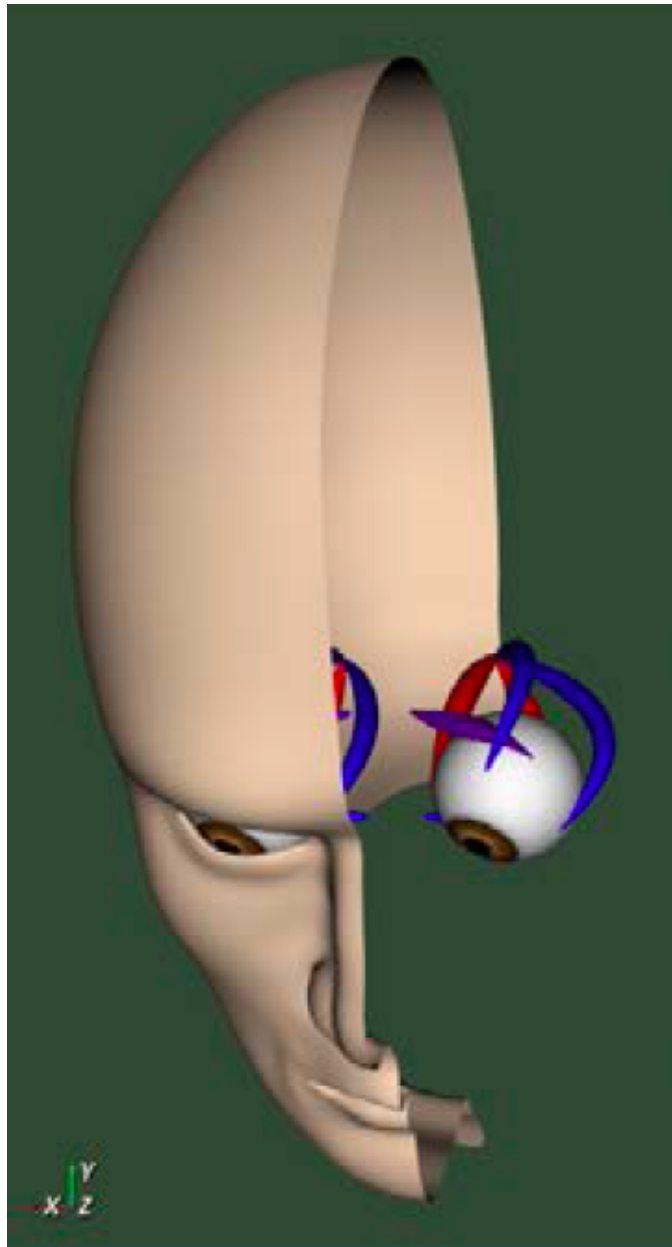


**Figure 2.** Example of the head model used.

455 number of inputs and outputs and may be written in C, C++, Python or MATLAB. The Cope-Chambers-  
456 Prescott-Gurney model's components were hand written in C++ and MATLAB. A BRAHMS *SystemML* file  
457 describes how the different components connect together and how data is passed between them (Mitchinson  
458 et al., 2010). The main BRAHMS program first reads the SystemML file, then dynamically loads all the  
459 required components before executing the system.

460 In the current work, the Cope-Chambers-Prescott-Gurney model was reproduced using the declarative  
461 SpineML markup language (Alex Cope and Paul Richmond, 2014; Richmond et al., 2014), with the help  
462 of the graphical SpineML model editing software called SpineCreator (Cope et al., 2015, 2016). SpineML,  
463 which is a development of the NineML specification (INCF Task Force on Multi-Scale Modeling, 2011),  
464 describes neural populations and their projections in a highly structured format in which neuron bodies, pre-  
465 and post-synapses are described in terms of *SpineML components*. These are similar to the components

466 provided by BRAHMS, but in this case, the components are an XML description of the functionality  
467 of the component, rather than a programmatic implementation, with one XML file per component. A  
468 SpineML *network layer* file then describes which components are used in the model, and how they are  
469 connected together. Finally, a number of SpineML *experiment layer* files specify how the model described  
470 in the network layer can be executed. In the experiment layer, the execution duration and timestep can be  
471 specified, along with input conditions, connection lesions and component parameter updates. A description  
472 of SpineML is given in Richmond et al. (2014); the definitive definition is found in the schemas (Cope  
473 et al., 2014). SpineCreator, in its rôle as a graphical editor for the SpineML format, was used to generate  
474 the SpineML files describing the model. It was also used to generate the diagrams of the model.

475 As a declarative format for model specification, SpineML is agnostic about how the model is executed. A  
476 number of simulation engines can be utilised, including DAMSON (Richmond, 2015), GeNN (Nowotny,  
477 2011; Nowotny et al., 2014) and BRAHMS (used here). The simulation engine incorporating BRAHMS is  
478 called SpineML\_2\_BRAHMS (Cope and James, 2015). SpineML\_2\_BRAHMS is a collection of XSLT  
479 stylesheets which first generate and compile C++ BRAHMS components from the SpineML component  
480 layer description files. SpineML\_2\_BRAHMS then uses the SpineML network and experiment layer files  
481 to generate a BRAHMS SystemML description of the model. Finally, SpineML\_2\_BRAHMS executes the  
482 model, now described entirely as a BRAHMS system, via a call to the BRAHMS binary. A number of  
483 additional hand-written components are present in SpineML\_2\_BRAHMS providing the inputs (constant  
484 inputs, time-varying inputs, etc) which the modeller specifies in the experiment layer.

485 In addition to the brain model components, all of which are code-generated using SpineML\_2\_BRAHMS as  
486 described above, two hand-written components are integrated into the model: The biomechanical eye model  
487 and a sensory input component. The sensory input component takes the eye's rotational state and the state  
488 of the experimental luminances and projects a retinotopic activity map into the brain model. Both of these  
489 BRAHMS components were hand-written in C++. To incorporate these components into the SpineML  
490 model, a SpineML\_2\_BRAHMS *external.xsl* file was used. The external.xsl file scheme for incorporating  
491 external BRAHMS components into a SpineML model was a new SpineML\_2\_BRAHMS feature motivated  
492 by the current work. Fig. 10 shows the workflow, in which the model specification files (blue box - a  
493 combination of SpineML files and C++ code), are processed (green box) into a BRAHMS system (red  
494 box).

495 Finally, numerical integration of the biomechanical eye model is based on the Kutta-Merson integration  
496 method.

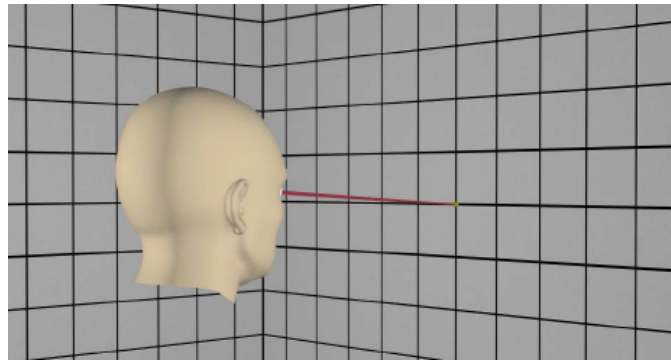


**Figure 3.** Example of the experimental set-up.

497     Figure 3 illustrates an example of the experimental set-up of the proposed framework, while Figures ??  
 498 and 5 depict the developed eye oculomotor simulation system.

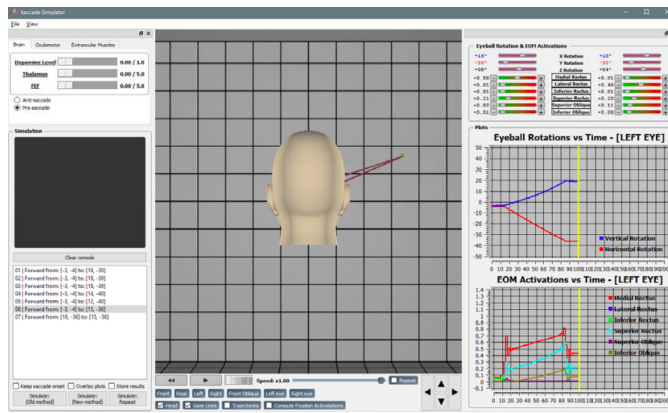


**Figure 5.** Example of use of the eye simulator system.

## 499     **2.6 Integrating the models and closing the loop**

500     The Cope-Chambers-Prescott-Gurney model closed its loop by passing the centroid of activity in SC\_deep  
 501 (once it had surpassed a threshold) back to the code that controlled the world, which would then use this  
 502 location to instantaneously change the model's view of the world. In our extended model, it was necessary  
 503 to connect the output of the brain model back to its input via the saccadic burst generator model and the  
 504 biomechanical eye. The resulting state of the eye, rather than the centroid of the superior colliculus, was  
 505 used to compute the input to the brain, given the luminances visible in the world.

506     A number of studies have considered the form of the connection between the deeper layers of the superior  
 507 colliculus and the saccadic burst generator (Van Gisbergen et al., 1985; Ottes et al., 1986; Waitzman et al.,  
 508 1991; Groh, 2001; Arai et al., 1994; Goossens, 2006; Tabareau et al., 2007; van Opstal and Goossens, 2008;  
 509 Goossens and van Opstal, 2012), which has become known as the spatial temporal transform (STT). The  
 510 spatial aspect of the transform is thought to be implemented by a weight-mapping (Tabareau et al., 2007;  
 511 Arai et al., 1994) and we follow this idea. Arai and co-workers trained a 20x20 neural network model  
 512 of the superior colliculus to discover the weight map under the assumption of 2D Gaussian activation  
 513 profiles (Arai et al., 1994). The training approach of Arai et al. (1994) was not feasible in this study  
 514 due to the length of time required to run our model and its stochasticity, which meant multiple runs  
 515 of the model were necessary in order to generate output statistics. Tabareau et al. (2007) wrote down

516 a theoretical form of the weight map, which follows from the mapping of Ottes et al. (1986) and the  
 517 assumption of invariant 2D Gaussian activity profiles in SC. As they found it closely resembles the results  
 518 of Arai et al. (1994), and it is a simple formulation, we considered it as the means to generate the six  
 519 weight maps in our own model. One barrier to the use of the weight map in Tabareau et al. (2007) was the  
 520 Cope-Chambers-Prescott-Gurney model's violation of the *invariant integral hypothesis*. This states that  
 521 the number of spikes emitted by a neural element during a saccade (or in our model, the integral of the  
 522 neuron's output during the saccade) should be a function only of its position within the hill of collicular  
 523 activity. That is, for any time-dependent hill of activity  $\mathcal{A}(\mathbf{z}, t)$  at  $\mathbf{z} = (r, \phi)$  on the collicular surface, the  
 524 integrated activity  $A_{\mathbf{x}}$  in an element at a vector  $\mathbf{x}$  away from  $\mathbf{z}$  is

$$A_{\mathbf{x}} = \int_t \mathcal{A}(\mathbf{z} - \mathbf{x}, t) dt \quad (22)$$

525 which is invariant for all  $\mathbf{z}$ . However, the very mapping on which the Tabareau et al. (2007) result is based  
 526 leads to a very *variant* activity profile in the Cope-Chambers-Prescott-Gurney model. A luminance of a  
 527 given size which excites activity near to the fovea causes activity in a large number of neurons, whereas  
 528 activity far from the fovea excites a much smaller region. This effect is clearly demonstrated in Fig. 8 for  
 529 equal sized targets both on and distal from the fovea.

530 This led us to hypothesise that the retinotopic mapping be accompanied by an associated widening  
 531 projection field such that the hill of activity in superior colliculus is invariant with position on the collicular  
 532 surface. There are a number of locations in the system in which this widening projection field could exist.  
 533 It could be implemented in the projections between the retinal populations and the superficial layer of  
 534 SC along with the projection between the World and the FEF population. However, this would affect  
 535 activity within the basal ganglia of the model, contradicting a result in Cope et al. (2017) which explains  
 536 the 'hockey stick' profile for saccade latency as a function of saccade eccentricity. Instead, we suggest  
 537 that a widening projection field is encoded within the superior colliculus itself, a complex, multi-layered  
 538 structure which could quite plausibly support such a function. Indeed, such widening activity can be seen in  
 539 the stimulation experiments in Vokoun et al. (2010) and Vokoun et al. (2014). In Ghitani et al. (2014), from  
 540 the same research group, evidence is presented for an excitatory and widely projecting pathway from the  
 541 stratum griseum intermediale (equivalent to our SC\_deep) to the more superficial layers stratum opticum  
 542 and stratum griseum superficiale. Although this pathway is a 'wide' projecting field, the experiments do  
 543 not indicate whether the projection *widens* along the rostral-caudal axis of the SC. Bayguinov et al. (2015)  
 544 presents evidence for another projecting field within SC whose connectivity pattern *does* change along  
 545 the rostral-caudal axis. This projection is inhibitory in nature. Although neither of these results precisely  
 546 match the widening, excitatory projection field hypothesised here, they do indicate that such connection  
 547 patterns are plausible. Although in this work we do not model the SC in detail, we extended the model with  
 548 a third functional layer named SC\_deep2, shown in Fig. 11 (Cope-Chambers-Prescott-Gurney has only the  
 549 two layers SC\_sup and SC\_deep). We introduced a widening projection based on a Gaussian projection  
 550 field whose width,  $\sigma(r)$  varies in inverse proportion to the magnification factor,  $M(r)$ , given in Eq. 12  
 551 according to:

$$\sigma(r) = \frac{m_\sigma}{M(r)} - \frac{m_\sigma}{M^0} + \sigma_0 \quad r > r_0 \quad (23)$$

552  $m_\sigma$  is a scalar parameter which determines the 'magnitude of the widening'.  $M^0$  is the 'starting' magni-  
 553 fication factor; within the foveal region ( $0 \leq r \leq r_0$ ), the projection field is not allowed to widen and

554 so

$$\sigma(r) = \sigma_0 \quad r \leq r_0 \quad (24)$$

555 which makes  $\sigma_0$  the width of the Gaussian projection field within the foveal region. (Note that the value  
 556 chosen for the width of the foveal region,  $r_0$  is not identical to the foveal shift parameter used in the  
 557 *DecayingAtFovea* projections into striatum.) The *Widening Gaussian* projection weight,  $w(r, d)$  is then  
 558 computed as:

$$w(r, d) = e^{-\frac{d^2}{2\sigma(r)^2}} \quad (25)$$

559 where  $d$  is the distance between the source and destination elements in the collicular plane.  $m_\sigma$  was set to  
 560 50,  $\sigma_0$  was 0.3,  $M^0$  was 12.43 and  $r_0$  was 20.

561 A further issue regarding the use of the theoretical weight map in Tabareau et al. (2007) was that it does  
 562 not consider the existence of the oblique extraocular muscles. There is evidence that only two dimensional  
 563 information is encoded in superior colliculus (Wurtz and Goldberg, 1972; Hepp et al., 1993; Van Opstal  
 564 et al., 1991), but the eye is actuated by six extraocular muscles. In order to find out a possible form for the  
 565 input to the oblique muscles we carried out a training process which depended on a centroid computation  
 566 in SC\_deep. For the four rectus muscles, the resulting weight maps resembled those found by Arai et al.  
 567 (1994). The trained maps for the oblique muscles had a form very close to those for the inferior and  
 568 superior rectus channels, but with a smaller magnitude. The inferior oblique map resembled the superior  
 569 rectus map and the superior oblique map resembled the inferior rectus. When parameterising the theoretical  
 570 weight maps, we set the inferior/superior oblique maps to be 1/10<sup>th</sup> of the superior/inferior rectus maps,  
 571 respectively. Interestingly, this suggests that there is a built-in synergy between the vertical and oblique  
 572 channels in the eye, although the results will show there is some systematic change in the oblique error  
 573 with saccade end-point location.

574 Tabareau et al. (2007) give a formulation for the weight maps in which it is possible to project both a  
 575 positive and a negative weight. In our model, all projections from SC\_deep are excitatory. This means that  
 576 each channel has a weight which follows the form:

$$w(r, \phi) = i e^{jr} \sin \left( \frac{2\pi\phi}{W_{nfs}} + k \right) \quad (26)$$

577 where  $i$ ,  $j$  and  $k$  are per-channel parameters for the weight maps.  $k$  is determined by the mapping. Only the  
 578 positive part of the sine is utilised.  $i$  and  $j$  are parameters to be found.

579 The saccadic burst generator model was originally conceived with the assumption of a step input, which  
 580 returns to zero activity at a suitable time to curtail the saccade and avoid staircase saccades (Gancarz and  
 581 Grossberg, 1998). In our model there is no such mechanism to reduce activity in SC\_deep, and elsewhere.  
 582 Although a successful, accurate saccade towards a target luminance will remove the excitation which caused  
 583 the activity in SC\_deep by bringing the target luminance within the masked, foveal region, the activity  
 584 in SC decays too slowly to avoid additional saccadic movements. We found it necessary to hypothesise  
 585 an inhibitory feedback mechanism from the SBG to the brain model. This is shown in Fig. 9, which  
 586 indicates how the output from the inhibitory burst neurons (IBN) of the SBG model are used to feed back  
 587 an inhibitory signal to the SC\_deep, thalamus and FEF populations in the brain model, resetting them ready  
 588 for the next saccade.

589 The output signals from the six channels of the SBG were connected to the six motoneuron inputs of the  
 590 biomechanical eye. The signal was normalised; a value of 1 meaning that all the motoneurons in the output

591 population were firing at their maximum rate and the force exerted by the relevant extraocular muscle  
592 was maximal. Channels innervated extraocular muscles as follows: Up: superior rectus; Down: inferior  
593 rectus; Right: medial rectus; Left: lateral rectus; Z+: superior oblique; Z-: inferior oblique. Because the  
594 medial rectus induces a rightward rotation of the eye, our single virtual eye is a *left* eye. The OpenSim  
595 implementation of the biomechanical eye was ‘wrapped’ (in the software sense) in a BRAHMS component.  
596 This made it possible to integrate the OpenSim model into the BRAHMS framework. The wrapper ensured  
597 that the input and output signals were correctly transferred and, importantly, handled the disparity in the  
598 solver timesteps used in the OpenSim model (25 ms) and the neural model (1 ms). This was achieved by  
599 having the BRAHMS wrapper create a separate thread to run the OpenSim model. The BRAHMS wrapper  
600 component was called on each 1 ms timestep, receiving the instantaneous activations from the motoneurons  
601 in the SBG. These activations, and the current simulation time, were written into a shared memory area,  
602 accessible by the OpenSim thread. Running independently, the OpenSim thread would update its inputs  
603 (using the most recent values in the shared memory area) whenever the simulation time had increased  
604 by 25 ms. It would then recompute its outputs (the rotational state of the eye) and write these into the  
605 same shared memory. The BRAHMS wrapper would update its outputs whenever they were changed in  
606 the shared memory by the OpenSim thread. A direct connection of the six outputs of the BRAHMS eye  
607 model component to the six inputs of the worldDataMaker BRAHMS component was specified in the  
608 SpineML\_2\_BRAHMS external.xsl file.

609 The eye model outputs its rotational state at each timestep. The rotational state is used to compute  
610 the view of the world in the eye’s frame of reference. To simplify the calculation, the luminances exist  
611 on a spherical surface at the centre of which is the eye. A hand-coded BRAHMS component called  
612 worldDataMaker computes the projection of the luminances into the eye’s frame of reference and then  
613 converts this representation into a retinotopic map to pass into the brain model. The input to the brain  
614 model is thus able to change continuously, on every timestep, rather than in a step-wise fashion when a  
615 saccade occurs, as in the Cope-Chambers-Prescott-Gurney model.

616 In the worldDataMaker BRAHMS component, the rotational state of the eye was used to construct  
617 Euler rotation matrices which transformed between the world’s frame of reference and the eye’s frame of  
618 reference. The worldDataMaker component received a specification of the world luminances in a JSON  
619 file called luminances.json at the start of each simulation. luminances.json specified the position, shape,  
620 size, luminance, appearance time and disappearance time of an arbitrary number of luminances. With this  
621 information, the instantaneous rotational state of the eye and the parameters of the retinotopic transform, it  
622 was able to compute the instantaneous input to the brain model.

623 The final models, on which the results of this paper are based are named ‘TModel3’, ‘TModel4’ and  
624 ‘TModel5’. Descriptions of these, and earlier versions of the model can be found in the code repository  
625 given in SUPPLEMENTAL DATA.

### 3 RESULTS

#### 626 3.1 Weight maps

627 We found the best parameters for the exponential in Eq. 26 ( $i$  and  $j$ ) by a manual tuning process. After  
628 selecting values for  $i$  and  $j$  in either the horizontal or vertical/oblique channels, we ran the model 6 times  
629 at each of 8 target eccentricities ( $7^\circ$ – $14^\circ$ ) which were purely in the direction of the newly parameterised  
630 channel. The training saccades were produced as described below in Sect. 3.3, with the same fixation  
631 and target luminances (crosses of magnitude 0.2 and 0.3) but with the fixation offset and target onset

632 occurring at 0.2 s. We measured the end-point of the saccade by detecting the location at which the saccade  
 633 velocity had dropped below 0.005 of its peak. We iterated until the mean saccade endpoint plotted versus  
 634 target was close to the ideal straight line—see Fig. 12(a) & (b). We applied the same parameters to both  
 635 directions of each channel;  $i_{up} = i_{down} = 0.00195$ ,  $j_{up} = j_{down} = 0.075$ ,  $i_{left} = i_{right} = 0.0016$  and  
 636  $j_{left} = j_{right} = 0.067$ .

637 The resulting weight maps (where the oblique maps are 1/10<sup>th</sup> of the vertical maps, as described earlier)  
 638 are shown in Fig. 13. First, recall that the  $r$  axis of the neural surface corresponds to the amplitude of a  
 639 saccade and the  $\phi$  axis indicates the polar direction of the saccade, as described in Sect. 2.2.2 and Fig. 8.  
 640 Fig. 13(a) shows the weight map for the muscle which rotates the eye to the left. As we modelled a left  
 641 eye, this actuates the lateral rectus muscle. The exponential rise of Eq. 26 is seen in the  $r$  direction; as  $r$   
 642 increases, so the connection strength to the SBG channel rises exponentially. The connection strength is  
 643 greatest along the centre line, for a value of  $\phi$  which corresponds to a purely leftward movement. Note that  
 644  $\phi$  is presented in neural coordinates, and not in degrees or radians;  $1 \leq \phi \leq 50$  corresponds to a range of  
 645 0° to 360°;  $\phi = 38.5$  corresponds to movements left. The connections strength drops away sinusoidally  
 646 as  $\phi$  moves away from the centre line at  $\phi = 38.5$ . In regions of the map for which there is no leftward  
 647 movement, that is, in the half of the map which corresponds to any movement with a rightward component,  
 648 the ‘left’ weight map is 0. Fig. 13(d) shows the weight map for rightward movements, actuating the medial  
 649 rectus muscle of the eye. The line of maximum connection strength is along  $\phi = 13.5$ . The map is a mirror  
 650 of Fig. 13(a), reflected about the line  $\phi = 26$ . The ‘left’ and ‘right’ weight maps are orthogonal; the non-zero  
 651 region of the ‘left’ map is zero in the ‘right’ map and vice versa. Fig 13(b) & (d) show the weight maps  
 652 for downward and upward eye movements; the ‘down’ map activates the SBG channel for the inferior  
 653 rectus muscle, the ‘up’ map activates the superior rectus. Note that ‘down’ is not orthogonal either to ‘left’  
 654 or ‘right’ because a saccade down and left is achieved by simultaneously activating both the lateral and  
 655 inferior rectus muscles. However, the ‘up’ map is orthogonal to the ‘down’ map and spans the edges of  
 656 the surface where  $\phi$  rolls over from 1 to 50. The line of maximum connection strength for the ‘up’ map is  
 657 along  $\phi = 1$ ; for ‘down’  $\phi = 26$ . Based on the training described in Sect. 2.6, the maps driving the superior  
 658 oblique (‘Z+’) and inferior oblique (‘Z-’) muscles were set to 1/10<sup>th</sup> of the ‘down’ and ‘up’ maps.

### 659 3.2 Saccade accuracy

660 In Fig. 12, we showed the result of running the model to targets located on the principle axes, on which  
 661 the model was trained. We then simulated single saccades to targets in one hemifield of the eye’s field of  
 662 view, with eccentricities between 6° and 14.5°. As in the training, we ran the simulation 6 times for each  
 663 target,  $\theta^t = (\theta_x^t, \theta_y^t, 0)$  to obtain mean saccade end-points. Fig. 14 shows saccade accuracy results for an  
 664 entire hemifield in the naïve model which passed the output of SC\_deep directly to SBG via the weight  
 665 maps. The ratio of the magnitude of the error vector to the magnitude of the target vector is plotted using a  
 666 colour map. This ratio is shown for the full, three dimensional error vector in Fig. 14(a) and for the  $x$ ,  $y$   
 667 and  $z$  components in Figs. 14(b)–(c). Inspection of Fig. 14(a) shows that the end-point error is minimal  
 668 along the principle axes ( $\theta_x^t = 0$  or  $\theta_y^t = 0$ ) and maximal near the 45° oblique targets (blue lines) with the  
 669 end point error as high as 80% of the programmed saccade magnitude. The  $x$  component error map in  
 670 Fig. 14(b) shows the same trend, mirrored about the ‘Target X’ axis, whereas the  $y$  and  $z$  component errors  
 671 are, relatively, much smaller. Because the  $x$  component of the error is clearly contributing to end point  
 672 errors which would not be considered ‘on target’, especially for oblique saccades, we considered the effect  
 673 of the non-uniform size of the hill of activity in SC\_deep.

674 In our model, the location, size and shape of activity in FEF, the basal ganglia, thalamus and superior  
675 colliculus is eccentricity dependent, in line with the retinotopic mapping stated by Ottes et al. (1986). More  
676 eccentric targets generate reduced activity, because fewer retinal neurons are excited far from the fovea.  
677 Cope et al. (2017) showed that this relationship can explain increased saccadic latencies for distal targets,  
678 resulting from reduced activity in the decision making circuitry of the basal ganglia. However, the notion  
679 that activity in superior colliculus is eccentricity-dependent conflicts with the result of Tabareau et al. (2007),  
680 who showed that an invariant hill of activity was required if this complex logarithmic weight mapping was  
681 to be used to drive a two-degree-of-freedom saccadic burst generator, and also with experimental findings,  
682 which do not show significant eccentricity dependence, at least in the burst layer (Anderson et al., 1998).

683 To bring our model in line with these results, whilst maintaining the eccentricity dependent activity in  
684 basal ganglia, we hypothesised that a ‘widening projection’ exists between two maps in superior colliculus.  
685 As described in Sect. 2.6, there is now experimental evidence for similar projections (Ghitani et al., 2014;  
686 Bayguinov et al., 2015) making this a plausible suggestion. Activities in one SC\\_deep layer remains  
687 eccentricity-dependent, with loops back to thalamus and cortex and through basal ganglia. This activity  
688 is then fed through a projection, which applies a Gaussian projection field, whose width increases with  
689 increasing stimulus eccentricity according to Eq. 25. The activity in this second SC\\_deep layer is then fed  
690 to the weight maps of the SBG. This model was called ‘TModel4’. TModel4 was parameterised such that  
691 its horizontal and vertical error was similar—so that its equivalent of Fig. 12 showed a similar sum of  
692 squares error.

693 Figs. 15(a)–(d) show the percentage errors for TModel4. First of all, note that the error magnitudes  
694 are much smaller. The mean errors are smaller for every axis. The largest errors produced by the model  
695 are approximately 15%, which are within the boundaries of what some authors have suggested would be  
696 regarded as an accurate saccade (McPeek and Keller, 2002; McPeek, 2006). The magnitude of the largest  
697 error vector is approximately 1.5°.

698 This result indicates that the exponential part of the Ottes et al. weight map from SC to the SBG cannot on  
699 its own compensate for the eccentricity-dependent size of the hill of activity. The introduction of a widening  
700 projection field substantially improves the mean accuracy of saccades across the field of view. We therefore  
701 suggest that the transformation between retinotopically mapped activity, and eccentricity-independent  
702 activity width occurs within the superior colliculus and works alongside a simple, monotonically increasing  
703 weight map between SC and the SBG channels.

### 704 3.3 Single saccades

705 Having finalised the model by setting the weight maps, we then proceeded to exercise the model  
706 (TModel4), starting with saccades to a single target; prosaccades. Fig. 16(a) shows 9 representative  
707 saccades to a single target luminance. Initially, the eye had rotational state  $\theta_x = \theta_y = \theta_z = 0$  with  
708 its fovea directed at a fixation luminance cross (span 6°, bar width 2°) of magnitude 0.2 (in arbitrary  
709 units). At a simulation time of 0.4 s, the fixation luminance was set to 0 and a target luminance cross  
710 of the same dimensions as the fixation but with magnitude 0.3 was illuminated at one of the 9 different  
711 locations, marked by crosses in Fig. 16(a). The resulting trajectories are plotted, with colour indicating the  
712 relationship between trajectories and target crosses. The approximate end-point error is visible in this figure,  
713 although the last point in each trajectory is the saccade position at 0.8 s and not the velocity-based end-point  
714 described above. Figs. 16(b) and (c) show the rotational components of the blue and red trajectories in  
715 Fig. 16(a) along with the target and fixation luminance values. Rotations are the eye’s Euler rotational  
716 components in the world frame of reference.

### 717 3.4 Saccade Latencies

718 To verify that our implementation of the brain model has the same functionality as that reported in Cope  
719 et al. (2017), we investigated the effect on saccadic response times of: target eccentricity; and any gap  
720 or overlap between fixation off-time and target on-time. We showed that the full model reproduces the  
721 ‘hockey stick’ shape shown in Fig. 7 of Cope et al. (2017) for horizontal [Fig. 17(a)], vertical [Fig. 17(b)]  
722 and oblique saccades (not shown). The latency increases with eccentricity far from the fovea because  
723 the retinotopic mapping reduces the activity in the basal ganglia for more eccentric targets (this effect is  
724 described in detail in Cope et al. (2017)). Closer to the fovea, the interaction between the foveal mask and  
725 the activity in FEF again leads to reduced input into the basal ganglia and an increased time to achieve  
726 disinhibition in SNr.

727 Fig. 17(c) shows latencies achieved when varying the time between fixation offset and target onset. This  
728 is termed the *gap condition*; and is represented by a scalar value which, if positive, refers to a gap between  
729 fixation offset and target onset, and when negative, signifies an overlap, with the fixation luminance  
730 persisting past the time at which the target is illuminated. A negative gap is also termed an *overlap*. Again,  
731 we verify the behaviour presented in Cope et al. (2017), explained as resulting from the inhibition of  
732 the cortico-thalamic loop by SNr. In the gap condition, when the fixation luminance is removed, activity  
733 in STN immediately begins to decay, allowing SNr activity to reduce and thereby reducing inhibition  
734 on thalamus, allowing the target luminance to build up quickly in FEF, thalamus and through the basal  
735 ganglia’s striatum and SNr. The shape of the curves in Fig. 17(c) matches the results in Cope et al. (2017)  
736 for target luminances of 1 and 0.6; for overlaps longer than 100 ms (gap < -100 ms), the latency becomes  
737 constant; the saccade is programmed whilst the fixation is present, with the target luminance inducing  
738 sufficient activity in striatum to ‘break through’ the SNr inhibition caused by the fixation. If the target  
739 luminance is reduced to 0.3, the balance is altered in favour of the fixation and the latency vs. gap becomes  
740 approximately linear and equal to the overlap time plus around 100 ms.

741 Fig. 17(d) shows the effect of the dopamine parameter on saccade latencies in gap, step and overlap  
742 conditions. In general, the effect of decreasing the dopamine parameter was a smooth, monotonic and  
743 undramatic increase in saccade latency. However, the data for the overlap condition with a target luminance  
744 which was 3 times as bright as the fixation luminance was more interesting. Here we see a transition around  
745 a dopamine value of 0.7. Below this value, the basal ganglia is not able to select the target luminance until  
746 the fixation is removed, reducing the excitatory drive from STN to SNr, and consequently the inhibition  
747 from SNr to the thalamo-cortical loop. For the target luminance 0.6, 0.7 dopamine allows the basal ganglia  
748 to select sufficiently well so that the target can build up in the thalamo-cortical loop, in spite of the fixation  
749 overlap.

750 The relationship between latency and the target luminance is given in Fig. 17(e). This shows latency for a  
751 100 ms gap, step and 100 ms overlap conditions for a given fixation luminance of 0.2, and a horizontally  
752 located target at  $\theta_y^t = -10^\circ$ . For the gap condition, we see very short latencies for luminances of about  
753 0.75 and above. Finally, the activity driving these express saccades is initiated by high firing rates in the  
754 superficial layer of SC (SCs), which then drives activity in thalamus and through the basal ganglia. A  
755 gradual transition from express saccades to reflexive saccades is observed as the contribution of the SCs  
756 becomes weaker and the drive from FEF into the thalamo-cortical loop becomes necessary to elicit a  
757 saccade. A similar gradual transition, albeit for higher latencies is seen for the step condition. At higher  
758 target luminances, the SCs has a greater effect on the activity in the thalamo-cortical loop. However, the  
759 activity in STN caused by the fixation luminance increases the latency at all luminance values compared  
760 with the gap condition. The overlap condition leads to increased latencies for luminances below 2.5, but

761 meets the step condition above this value, at which the 0.2 fixation luminance appears to have a negligible  
762 effect on the system.

### 763 3.5 Saccade sequences

764 We now present results derived from the fully parameterised and integrated model; where we took  
765 advantage of the fact that it is a closed loop system. This allowed us to present sequences of target  
766 luminances and allow the model to direct its fovea at the most salient target.

#### 767 3.5.1 Out & return

768 We investigated the behaviour of the model for saccade sequences. In one experiment, we illuminated  
769 a fixation cross from 0 s until 0.4 s, followed by a target at (0, -10°) from 0.4 s until 0.8 s. Finally, the  
770 fixation was again shown from 0.8 s until the end of the simulation at 2 s. This induced a saccade to a  
771 10° eccentricity, followed by a return saccade back to the null point. We noticed some irregularities in  
772 the return saccades, which **were accurate**, but had a significant overshoot. More perplexingly, if the target  
773 was switched repeatedly between 0° and 10°, second and subsequent *outward* saccades also showed this  
774 overshoot. We found that the cause of these irregularities was the lack (in ‘TModel4’) of any mechanism to  
775 reset the tonic neurons in the SBG after the first saccade. This resulted in TN activity in the left channel  
776 *and also* in the right channel. Interestingly, this ensured that, at least for a few, consecutive out-and-return  
777 saccades, the saccade accuracy was accidentally relatively good, with trajectories resembling experimental  
778 data (Bahill and Stark (1979), p. 6). **Had the return accuracy not been so accurate, we may have noticed the  
779 lack of a tonic neuron reset mechanism and corrected this oversight earlier.** Such a mechanism is indeed  
780 proposed and included in the connectivity of the Gancarz and Grossberg (1998) model. We implemented  
781 this feature by adding an additional inhibitory input to the ‘integrator’ component of TModel4, driven  
782 by the contralateral EBN population, naming the new model ‘TModel5’. Now, when the eye is directed  
783 towards an eccentric target which is then exchanged with a target at the null point, the EBN activity toward  
784 the null point will tend to extinguish the TN activity which was holding the eye at the eccentric position.  
785 We verified that none of the single saccade results were affected by this modification.

786 Fig. 18 shows the outward and return trajectories produced by the experiment with the TN reset mecha-  
787 nism. Panel (a) shows the *x* and *y* rotation trajectory; panel (b) shows individual rotational components of  
788 the eye. Fig. 18(c) shows out and return trajectories for three other saccade targets; horizontal, vertical and  
789 oblique. The trajectories have characteristic shapes and also show some stochastic variation caused by the  
790 noise in the model [see dashed trajectories in Fig. 18(a)].

791 The return trajectories (magenta lines) showed a distinctly different form from the outward trajectories.  
792 They overshot their destination (the null point) significantly. This resulted from the removal of the TN  
793 activity which was holding the eye at the eccentric target location. Removal of this activity, and thus the  
794 static force exerted by the corresponding extraocular muscle, meant that the eye was subject both to a new  
795 muscular force towards the null point *alongside* the restorative spring force of the lengthened rectus muscle.  
796 This stands as a shortcoming of the model.

#### 797 3.5.2 Double steps

798 In another experiment, we probed the response of the model to double step stimuli of the type described  
799 in Becker and Jrgens (1979). In that work, the response of human subjects was investigated when shown  
800 stimuli at 15° and 30° eccentricity with variable delay between the stimuli. If the smaller eccentricity  
801 stimulus was shown first, followed by the more distal on the same side of the field of view, this was called  
802 a ‘staircase’ presentation. We carried out a ‘staircase’ presentation, shown in Fig. 19, where our small

803 eccentricity luminance was at 8° and our more distal luminance was at 12° (both to the right of centre). We  
804 found that there was a critical time delay between the luminances of about 30 ms. If they were presented  
805 with a delay smaller than this value, then a single, slightly hypermetric saccade was made. This response  
806 type is called a *final angle response*. A delay greater than 30 ms between the stimuli would lead to double  
807 step saccades (a so-called *initial angle response*), with the first saccade arriving at 8° (though with greater  
808 variability than normal), and a second saccade being made to a location hypometric of 12° after a pause  
809 of about 240 ms. Fig. 19(a) shows the mean trajectories from 5 simulations of the staircase doublestep  
810 presentation alongside the result for a single saccade to the final angle of 12°. Dash-dot lines show ±1  
811 standard deviation about the mean. The corresponding trajectories are shown in Fig. 19(b).

812 Inspection of the activity maps in FEF and SC\_deep (not shown) indicates that when the 8° target  
813 is illuminated for 30 ms or more, the activity associated with this target angle is able to dominate the  
814 activity, hence the execution of a reasonably accurate saccade. The inhibitory feedback from the SBG then  
815 extinguishes activity in FEF, thalamus and SC, which means that a full 200 ms or more is required to allow  
816 activity in these populations to build up again in order to make the smaller saccade from 8° to 12°. This is  
817 in contrast to experimental findings in which the corrective second saccade is often executed *more quickly*  
818 than if it were programmed on its own (Becker and Jrgens, 1979).

## 4 DISCUSSION

819 The aim of this study was to demonstrate the importance of modelling neurological systems *in concert with*  
820 the biomechanical systems with which they have evolved in parallel. We hypothesised that by combining  
821 existing neurophysiological models with an accurate model of a musculo-skeletal system, and then ‘closing  
822 the loop’ by allowing the movements of the virtual muscles to modulate sensory feedback to the brain model,  
823 shortcomings in the constituent models would be revealed, leading to new knowledge. To demonstrate the  
824 validity of this hypothesis, we built an integrated model and then identified the modifications which were  
825 necessary to give it the ability to make accurate movements under one type of stimulus. We then examined  
826 its behaviour with other stimuli.

827 We chose the oculomotor model as a basis for this study because it has only three degrees of freedom,  
828 making it one of the simplest musculo-skeletal systems. Furthermore, eye movements fall into several  
829 well-defined categories, each being controlled by separate brain circuits, we were therefore justified in  
830 modelling a system which produced only saccadic eye movements. Nevertheless, we are aware that we  
831 did not create a complete model of the system; no treatment of the cerebellum was attempted, justified  
832 because cerebellum appears to have only a minor effect on saccade accuracy (Dean and Porrill, 2008),  
833 probably correcting for slow to medium timescale changes in the physical dynamics of the eyeball (Dean  
834 et al., 1994).

835 To summarise our model integration: We combined the Cope-Chambers-Prescott-Gurney model (Cope  
836 et al., 2017) with a saccadic burst generator model based on the work of Gancarz and Grossberg (1998),  
837 using this to drive the input of a new biomechanical eye model. To achieve the spatial transformation from  
838 the retinotopic maps of the Cope-Chambers-Prescott-Gurney model to the six ‘muscle channel’ inputs  
839 for the saccadic burst generator, we used the mapping of Ottes et al. (1986) to produce parameterised  
840 weight maps along with an empirically discovered synergy for the torsional weight maps. We introduced an  
841 additional transformation to the brain model to achieve invariant sized hills of activity in superior colliculus  
842 to fulfil the invariant integral hypothesis of Tabareau et al. (2007). We closed the loop using a software  
843 component which transformed a view of a world containing luminous cross shapes into the eye’s frame

of reference, given its instantaneous rotational state. This component also computed the inverse of the mapping from Ottes et al. (1986) to project the view retinotopically into the brain model. This paper serves to describe how we achieved the integration in order to test our hypothesis, and we intend that the material and methods section, along with the model code itself, will help others to carry out similar studies. However, we wish to devote the majority of this discussion to what can be learned from an integrated model of a combined brain and biomechanical system, using our oculomotor system as an example.

Our integration approach revealed three ways in which this model fails to provide a full understanding of the saccadic system. In each case, the issue is made clear *as a result of the integration*. This is not to say that other approaches may not also reveal shortcomings; we will see that one of our cases has been independently identified (Groh, 2011).

#### 4.1 The need for a widening projection field

The original combination of the Cope-Chambers-Prescott-Gurney model with the theoretical weight maps of Ottes et al. (1986) and Tabareau et al. (2007) resulted in a model which was able to produce accurate saccades only along the principle rotational axes (Fig. 14). Thus, *the integration of the models* suggested that an additional layer was required to achieve accurate saccades for oblique, as well as for horizontal and vertical saccades. Although the *need* for an invariant integral is discussed in Tabareau et al. (2007) as resulting from their theoretical study, the mechanism by which such an invariant Gaussian hill is generated is not. By combining the models, we were forced to consider this mechanism, and hypothesised that a widening projection field would be a candidate mechanism. The results of Fig. 15 indicate that a substantial improvement in accuracy is indeed achieved by this new mechanism.

#### 4.2 Saccades from non-null starting positions

The implementation of a biophysically accurate model of the eye, and the closed-loop nature of the model makes it very natural to consider how the model will behave making saccades from arbitrary starting positions, or how it would respond to a sequence of stimuli. This was the motivation for the out-and-return experiment (Fig. 18) as well as for the double step experiment (Fig. 19). We found that return saccades were substantially affected by the biomechanics of the eye, as the brain and brainstem model had no mechanism to account for the position-dependent restoring forces applied by the eye. This question has been addressed by other authors; Groh (2011) investigates the effect of initial eye position on stimulated saccades and finds a need for the signal in superior colliculus to be modulated by an eye position signal. Ling et al. (2007) shows the existence of a position dependent firing rate offset in abducens neurons. Though we will not speculate here on the mechanism by which return saccades may be made accurate whilst also resetting the activity of tonic neurons in the SBG, it is interesting that in the model in which we omitted to reset TN activity (TModel4), we obtained relatively accurate out-and-return saccades which closely resembled experimental data. We suggest that residual activity in TN populations may offer an explanation for how the restorative force exerted by the elastic oculomotor muscles is compensated for. A comparison of this idea with that of Groh (2011) (that there is a modulation, from a brainstem signal, of the SC readout) would make a subject for a future study. Although these existing studies have highlighted this issue, the inaccurate return saccades which the model makes from eccentric starting positions provide a clear example of the way in which integrating known models into a closed-loop system can highlight deficiencies in the model.

#### 4.3 Inhibitory feedback from saccadic burst generator to brain

The third issue raised by the integration of the component models of the saccadic system has, like the return saccades, to do with resetting activity. In this case, rather than the reset of activity in the TN

population in the brainstem, it is the question of how the activity in the *brain* model should be reset after each saccade. When a target luminance is projected onto the World population in the model, this induces activity which ‘reverberates’ in loops through FEF, basal ganglia, SC and thalamus. The brainstem contains a mechanism to limit the timescale of a saccade (inhibitory feedback from EBN, via IBN to LLBN; see Fig. 9). However, if the activity in SC is not reset, then following the completion of the first saccade, a series of subsequent ‘staircase’ saccades will be executed. There needs to be a mechanism to extinguish activity in SC, but also in FEF and thalamus, as activity in either of these populations can build up and eventually cause repeat activity in SC and another saccade. We added hypothetical inhibitory feedback connections to our model, such that the IBN populations in the SBG would inhibit activity in FEF, thalamus and SC\_deep (Fig. 9), preventing the occurrence of staircase saccades.

An examination of the behaviour of the model when presented with ‘double-step stimuli’ reveals a problem with this scheme. We found that when double-step stimuli were presented (where an initial target at  $8^\circ$  was replaced with a  $12^\circ$  target after 30 or 40 ms) and a double saccade was made [Fig. 19(a), black lines] the second saccade latency was *longer* even than the initial saccade. This contrasts with Becker and Jrgens (1979) who find that second, corrective saccades occur with *shorter* latencies. This suggests that the inhibitory reset signal implemented in this model is too strong or has the wrong timescales. This issue highlights the fact that connections *between* component models are quite as important as the connections within each model.

#### 4.4 Concluding remarks

The omission of the cerebellum will not have escaped the reader’s notice. Whilst many of the nuclei known to be involved in the production of saccadic eye movements are incorporated within the model, the cerebellum is not. The cerebellum is known to play an important rôle in saccade programming (Dean et al., 1994; Schweighofer et al., 1996; Quaia et al., 2000; Kleine, 2003). It may be able to completely replace the functionality of the colliculus when lesioned (Aizawa and Wurtz, 1998; Lefvre et al., 1998). However, this rôle is typically considered to be one of accuracy tuning (Barash et al., 1999; Dean et al., 1994); operating as an additive model. Furthermore, saccades made by individuals with cerebellar ataxias perform with only moderate loss of saccade accuracy (Barash et al., 1999; Federighi et al., 2011). Because we did not address learning in our model, and because our aim was to demonstrate the utility of integrating brain with biomechanics in order to highlight deficiencies, we considered the omission of the cerebellar nuclei acceptable in the present work.

We have not addressed the question of saccade duration in this paper. Saccade duration is of interest in models which produce two (or three) dimensional saccades, because the dynamics of a saccade follow well known relationships with the saccade eccentricity, regardless of the saccade angle. This causes a problem for models (such as the present one) for which some of the dynamic behaviour is generated within orthogonal components. For example, saccade duration increases with target eccentricity. A  $10^\circ$  eccentricity oblique ( $45^\circ$  up and right) saccade is composed (approximately) of a  $7^\circ$  upwards component and a  $7^\circ$  rightwards component. If the component based model is responsible for the dynamics, then the  $10^\circ$  oblique saccade would be expected to have the dynamics of a  $7^\circ$  up or  $7^\circ$  right saccade. This is not found in practice, and the components are said to have been stretched, hence the name for this effect ‘component stretching’. The Gancarz and Grossberg (1998) model is reported to take account of the component stretching effect via the OPN neuron population. We did not find this effect in our implementation of the model; the duration of oblique saccades at a given eccentricity was always substantially different from the duration of the corresponding purely vertical or horizontal saccade. Because there is a somewhat complicated interplay

929 between the dynamics of the superior colliculus driving the dynamic system of the SBG, we feel this is  
930 outside the scope of the current work and a subject for a future paper.

931 This work represents a step forward in the modelling of neuromuscular systems, not because it sig-  
932 nificantly advances any of the constituent models, but because it *integrates* the models into a complete,  
933 *behaving* system. This is not the first integrated brain model composed of separately developed components.  
934 The works of N'Guyen et al. (2014) and Thurat et al. (2015) are both based on an example of a brain model  
935 which drives a simple, second order model of the eye. DeWolf et al. (2016) describes a reach model which  
936 integrates models of cortex and cerebellum to drive a two degree-of-freedom arm model. Both of these  
937 example systems nevertheless operate using 'curated' inputs supplied by the modeller.

938 In contrast, the current work allows the state of the system to determine the input delivered to the model.  
939 The modeller only curates the state of the world at each time point, but the actual input to the model  
940 depends on the eye's rotational state. This is, to our knowledge, the first model which integrates the brain  
941 with an accurate biophysical system and closes the loop in this way, enabling the system to reproduce  
942 behaviour. As such, it offers a platform for testing more complex saccadic behaviour such as antisaccades  
943 or saccades in the presence of distractor stimuli. We believe that by building closed loop systems which  
944 express behaviour, we, and others will develop a new field of *computational neurobehaviour*, which will  
945 share themes from neuroscience, artificial intelligence, decision science and embodied robotics.

## DISCLOSURE/CONFLICT-OF-INTEREST STATEMENT

946 The authors declare that the research was conducted in the absence of any commercial or financial  
947 relationships that could be construed as a potential conflict of interest.

## AUTHOR CONTRIBUTIONS

948 SJ, AB and AC implemented existing parts of the model in SpineML. AB developed the saccade generator  
949 brainstem model. SJ performed the technical and scientific integration of the biomechanical eye. CP and  
950 KM developed the biomechanical eye model. SJ wrote the manuscript; SA, AB, KG and KM contributed  
951 to the manuscript. KG conceived the project.

## ACKNOWLEDGEMENTS

952 *Funding:* European Union FP7 Grant 610391 'NoTremor'.

## SUPPLEMENTAL DATA

953 The model specification, results and all code required to reproduce the results of this work are available at:  
954 [https://github.com/ABRG-Models/OMM\\_NeuroMuscular](https://github.com/ABRG-Models/OMM_NeuroMuscular)

## REFERENCES

- 955 Aizawa, H. and Wurtz, R. H. (1998). Reversible inactivation of monkey superior colliculus. I. Curvature of  
956 saccadic trajectory. *Journal of neurophysiology* 79, 2082–2096  
957 Alex Cope and Paul Richmond (2014). SpineML. RRID: SCR\_015641  
958 Anderson, R. W., Keller, E. L., Gandhi, N. J., and Das, S. (1998). Two-dimensional saccade-related  
959 population activity in superior colliculus in monkey. *Journal of Neurophysiology* 80, 798–817

- 960 Arai, K., Keller, E., and Edelman, J. (1994). Two-dimensional neural network model of the primate  
961 saccadic system. *Neural Networks* 7, 1115. doi:10.1016/S0893-6080(05)80162-5
- 962 Bahill, A. T. and Stark, L. (1979). The trajectories of saccadic eye movements. *Scientific American* 240,  
963 108–117
- 964 Barash, S., Melikyan, A., Sivakov, A., Zhang, M., Glickstein, M., and Thier, P. (1999). Saccadic dysmetria  
965 and adaptation after lesions of the cerebellar cortex. *Journal of Neuroscience* 19, 10931–10939
- 966 Bayguinov, P. O., Ghitani, N., Jackson, M. B., and Basso, M. A. (2015). A Hard-Wired Priority Map  
967 in the Superior Colliculus Shaped by Asymmetric Inhibitory Circuitry. *Journal of Neurophysiology*  
968 doi:10.1152/jn.00144.2015
- 969 Becker, W. and Jrgens, R. (1979). An analysis of the saccadic system by means of double step stimuli.  
970 *Vision Research* 19, 967–983. doi:10.1016/0042-6989(79)90222-0
- 971 Bevan, M. D. and Wilson, C. J. (1999). Mechanisms underlying spontaneous oscillation and rhythmic  
972 firing in rat subthalamic neurons. *The Journal of neuroscience : the official journal of the Society for  
973 Neuroscience* 19, 7617–28
- 974 Blenkinsop, A., Anderson, S., and Gurney, K. (2017). Frequency and function in the basal ganglia: the  
975 origins of beta and gamma band activity. *The Journal of Physiology* doi:10.1113/JP273760
- 976 Bogacz, R. and Gurney, K. (2007). The basal ganglia and cortex implement optimal decision making  
977 between alternative actions. *Neural Computation* 19, 442–477. doi:10.1162/neco.2007.19.2.442
- 978 Bolam, J., Hanley, J., Booth, P., and Bevan, M. (2000). Synaptic organisation of the basal ganglia. *Journal  
979 of Anatomy* 196, 527–542
- 980 Brown, P., Oliviero, A., Mazzone, P., Insola, A., Tonali, P., and Di Lazzaro, V. (2001). Dopamine  
981 Dependency of Oscillations between Subthalamic Nucleus and Pallidum in Parkinson's Disease. *J.  
982 Neurosci.* 21, 1033–1038
- 983 Casteau, S. and Vitu, F. (2012). On the effect of remote and proximal distractors on saccadic behavior: A  
984 challenge to neural-field models. *Journal of vision* 12, 14
- 985 Chen, L. L. and Wise, S. P. (1995). Supplementary eye field contrasted with the frontal eye field during  
986 acquisition of conditional oculomotor associations. *Journal of Neurophysiology* 73, 1122–1134
- 987 Chevalier, G. and Deniau, J. M. (1990). Disinhibition as a basic process in the expression of striatal  
988 functions. *Trends in Neurosciences* 13, 277–280
- 989 Cope, A., Chambers, J. M., Prescott, T. J., and Gurney, K. N. (2017). Basal Ganglia Control Of  
990 Reflexive Saccades: A Computational Model Integrating Physiology Anatomy And Behaviour. *bioRxiv*  
991 doi:10.1101/135251
- 992 Cope, A. J. and James, S. S. (2015). SpineML\_2\_brahms (NoTremor Oculomotor branch)
- 993 Cope, A. J., Richmond, P., and Allerton, D. (2014). The SpineML toolchain: enabling computational neu-  
994 roscience through flexible tools for creating, sharing, and simulating neural models. *BMC Neuroscience*  
995 15, P224
- 996 Cope, A. J., Richmond, P., and James, S. S. (2015). SpineCreator. RRID: SCR\_015637
- 997 Cope, A. J., Richmond, P., James, S. S., Gurney, K., and Allerton, D. J. (2016). SpineCreator: a  
998 Graphical User Interface for the Creation of Layered Neural Models. *Neuroinformatics* doi:10.1007/  
999 s12021-016-9311-z
- 1000 Daniel, P. M. and Whitteridge, D. (1961). The representation of the visual field on the cerebral cortex in  
1001 monkeys. *The Journal of Physiology* 159, 203–221. doi:10.1113/jphysiol.1961.sp006803
- 1002 Dean, P. (1995). Modelling the role of the cerebellar fastigial nuclei in producing accurate saccades: the  
1003 importance of burst timing. *Neuroscience* 68, 1059–1077

- 1004 Dean, P., Mayhew, J. E., and Langdon, P. (1994). Learning and maintaining saccadic accuracy: a model of  
1005 brainstemcerebellar interactions. *Journal of Cognitive Neuroscience* 6, 117–138
- 1006 Dean, P. and Porrill, J. (2008). Adaptive filter models of the cerebellum: computational analysis. *Cerebellum*  
1007 7, 567–571
- 1008 Delgado, A., Sierra, A., Querejeta, E., Valdiosera, R., and Aceves, J. (1999). Inhibitory control of the  
1009 GABAergic transmission in the rat neostriatum by D2 dopamine receptors. *Neuroscience* 95, 1043–1048.  
1010 doi:10.1016/S0306-4522(99)00495-9
- 1011 DeLong, M., Crutcher, M. D., and Georgopoulos, A. (1985). Primate globus pallidus and subthalamic  
1012 nucleus: functional organization. *Journal of Neurophysiology* 53, 530–543
- 1013 Deubel, H. and Schneider, W. X. (1996). Saccade target selection and object recognition: Evidence for a  
1014 common attentional mechanism. *Vision Research* 36, 1827–1837. doi:10.1016/0042-6989(95)00294-4
- 1015 DeWolf, T., Stewart, T. C., Slotine, J.-J., and Eliasmith, C. (2016). A spiking neural model of adaptive arm  
1016 control. *Proceedings of the Royal Society B: Biological Sciences* 283, 20162134. doi:10.1098/rspb.2016.  
1017 2134
- 1018 Dorris, M. C., Par, M., and Munoz, D. P. (1997). Neuronal Activity in Monkey Superior Colliculus Related  
1019 to the Initiation of Saccadic Eye Movements. *The Journal of Neuroscience* 17, 8566
- 1020 Edelman, J. A. and Keller, E. L. (1996). Activity of visuomotor burst neurons in the superior colliculus  
1021 accompanying express saccades. *Journal of Neurophysiology* 76, 908
- 1022 Federighi, P., Cevenini, G., Dotti, M. T., Rosini, F., Pretegiani, E., Federico, A., et al. (2011). Differences  
1023 in saccade dynamics between spinocerebellar atrophy 2 and late-onset cerebellar ataxias. *Brain* 134,  
1024 879–891. doi:10.1093/brain/awr009
- 1025 Fuchs, A. and Luschei, E. (1970). Firing patterns of abducens neurons of alert monkeys in relationship to  
1026 horizontal eye movement. *Journal of Neurophysiology* 33, 382–392
- 1027 Funahashi, S., Chafee, M. V., and Goldman-Rakic, P. S. (1993). Prefrontal neuronal activity in rhesus  
1028 monkeys performing a delayed anti-saccade task. *Nature* 365, 753
- 1029 Galvan, A. and Wichmann, T. (2008). Pathophysiology of Parkinsonism. *Clinical Neurophysiology* 119,  
1030 1459–1474. doi:10.1016/j.clinph.2008.03.017
- 1031 Gancarz, G. and Grossberg, S. (1998). A neural model of the saccade generator in the reticular formation.  
1032 *Neural Networks* 11, 1159–1174. doi:10.1016/S0893-6080(98)00096-3
- 1033 Gaymard, B., Ploner, C. J., Rivaud, S., Vermersch, A. I., and Pierrot-Deseilligny, C. (1998). Cortical  
1034 control of saccades. *Experimental Brain Research* 123, 159–163. doi:10.1007/s002210050557
- 1035 Gerfen, C. R., Engbar, T. M., Mahan, L. C., Susel, Z., Chase, T. N., Monsma, F. J., et al. (1990). D1 and  
1036 D2 dopamine receptor regulated gene-expression of striatonigral and striatopallidal neurons. *Science*  
1037 250, 1429–1432
- 1038 Ghitani, N., Bayguinov, P. O., Vokoun, C. R., McMahon, S., Jackson, M. B., and Basso, M. A. (2014).  
1039 Excitatory Synaptic Feedback from the Motor Layer to the Sensory Layers of the Superior Colliculus.  
1040 *The Journal of Neuroscience* 34, 6822–6833. doi:10.1523/JNEUROSCI.3137-13.2014
- 1041 Gian G. Mascetti and Jorge R. Arriagada (1981). Tectotectal interactions through the commissure of the  
1042 superior colliculi. An electrophysiological study. *Experimental Neurology* 71, 122–133
- 1043 Girard, B. and Berthoz, A. (2005). From brainstem to cortex: Computational models of saccade generation  
1044 circuitry. *Progress in Neurobiology* 77, 215–251. doi:10.1016/j.pneurobio.2005.11.001
- 1045 Gonon, F. (1997). Prolonged and extrasynaptic excitatory action of dopamine mediated by D1 receptors in  
1046 the rat striatum in vivo. *The Journal of neuroscience : the official journal of the Society for Neuroscience*  
1047 17, 5972–8

- 1048 Goossens, H. (2006). Dynamic Ensemble Coding of Saccades in the Monkey Superior Colliculus. *Journal  
1049 of Neurophysiology* 95, 2326–2341. doi:10.1152/jn.00889.2005
- 1050 Goossens, H. and van Opstal, A. J. (2012). Optimal control of saccades by spatial-temporal activity patterns  
1051 in the monkey superior colliculus. *PLoS computational biology* 8, e1002508
- 1052 Groh, J. M. (2001). Converting neural signals from place codes to rate codes. *Biological cybernetics* 85,  
1053 159–165
- 1054 Groh, J. M. (2011). Effects of Initial Eye Position on Saccades Evoked by Microstimulation in the Primate  
1055 Superior Colliculus: Implications for Models of the SC Read-Out Process. *Frontiers in Integrative  
1056 Neuroscience* 4. doi:10.3389/fnint.2010.00130
- 1057 Gurney, K., Prescott, T. J., and Redgrave, P. (2001a). A computational model of action selection in the  
1058 basal ganglia. I. A new functional anatomy. *Biological cybernetics* 84, 401–10
- 1059 Gurney, K., Prescott, T. J., and Redgrave, P. (2001b). A computational model of action selection in the  
1060 basal ganglia. II. Analysis and simulation of behaviour. *Biological cybernetics* 84, 411–23
- 1061 Hallworth, N. E., Wilson, C. J., and Bevan, M. D. (2003). Apamin-sensitive small conductance calcium-  
1062 activated potassium channels, through their selective coupling to voltage-gated calcium channels, are  
1063 critical determinants of the precision, pace, and pattern of action potential generation in rat subthalamic  
1064 nucleus neurons in vitro. *The Journal of neuroscience* 23, 7525–7542
- 1065 Harsing, L. G. and Zigmond, M. J. (1997). Influence of dopamine on GABA release in striatum: evidence  
1066 for D1-D2 interactions and non-synaptic influences. *Neuroscience* 77, 419–29
- 1067 Hazy, T. E., Frank, M. J., and O'Reilly, R. C. (2007). Towards an executive without a homunculus:  
1068 computational models of the prefrontal cortex/basal ganglia system. *Philosophical Transactions of the  
1069 Royal Society B: Biological Sciences* 362, 1601–1613. doi:10.1098/rstb.2007.2055
- 1070 Hepp, K. and Henn, V. (1983). Spatio-temporal recoding of rapid eye movement signals in the monkey  
1071 paramedian pontine reticular formation (PPRF). *Experimental brain research* 52, 105–120
- 1072 Hepp, K., Van Opstal, A. J., Straumann, D., Hess, B. J., and Henn, V. (1993). Monkey superior colliculus  
1073 represents rapid eye movements in a two-dimensional motor map. *Journal of neurophysiology* 69,  
1074 965–979
- 1075 Hernndez-Lpez, S., Bargas, J., Surmeier, D. J., Reyes, A., and Galarraga, E. (1997). D1 receptor  
1076 activation enhances evoked discharge in neostriatal medium spiny neurons by modulating an L-type  
1077 Ca<sup>2+</sup> conductance. *The Journal of neuroscience : the official journal of the Society for Neuroscience* 17,  
1078 3334–42
- 1079 Hikosaka, O., Takikawa, Y., and Kawagoe, R. (2000). Role of the basal ganglia in the control of purposive  
1080 saccadic eye movements. *Physiological reviews* 80, 953–978
- 1081 Howard, L. A. and Tipper, S. (1997). Hand deviations away from visual cues: indirect evidence for  
1082 inhibition. *Experimental brain research* 113, 144–152
- 1083 INCF Task Force on Multi-Scale Modeling (2011). Network Interchange for Neuroscience Modeling  
1084 Language (NineML)
- 1085 Isa, T. (2002). Intrinsic processing in the mammalian superior colliculus. *Current Opinion in Neurobiology*  
1086 12, 668–677. doi:10.1016/S0959-4388(02)00387-2
- 1087 Isa, T. and Hall, W. C. (2009). Exploring the Superior Colliculus In Vitro. *Journal of Neurophysiology*  
1088 102, 2581–2593. doi:10.1152/jn.00498.2009
- 1089 James, S., Bell, O. A., Nazli, M. A. M., Pearce, R. E., Spencer, J., Tyrrell, K., et al. (2017). Target-distractor  
1090 synchrony affects performance in a novel motor task for studying action selection. *PLOS ONE* 12,  
1091 e0176945. doi:10.1371/journal.pone.0176945

- 1092 Kita, H. and Kitai, S. T. (1991). Intracellular study of rat globus pallidus neurons: membrane properties  
1093 and responses to neostriatal, subthalamic and nigral stimulation. *Brain research* 564, 296–305
- 1094 Kleine, J. F. (2003). Saccade-Related Neurons in the Primate Fastigial Nucleus: What Do They Encode?  
1095 *Journal of Neurophysiology* 90, 3137–3154. doi:10.1152/jn.00021.2003
- 1096 Khn, A. A., Williams, D., Kupsch, A., Limousin, P., Hariz, M., Schneider, G.-H., et al. (2004). Event-  
1097 related beta desynchronization in human subthalamic nucleus correlates with motor performance. *Brain*  
1098 : a journal of neurology 127, 735–46. doi:10.1093/brain/awh106
- 1099 Lefvre, P., Quaia, C., and Optican, L. M. (1998). Distributed model of control of saccades by superior  
1100 colliculus and cerebellum. *Neural Networks* 11, 1175–1190
- 1101 Linden, R. and Perry, V. (1983). Massive retinotectal projection in rats. *Brain research* 272, 145–149
- 1102 Ling, L., Fuchs, A. F., Siebold, C., and Dean, P. (2007). Effects of initial eye position on saccade-related  
1103 behavior of abducens nucleus neurons in the primate. *Journal of Neurophysiology* 98, 3581–3599
- 1104 Maes, P. (1989). *The dynamics of action selection* (Artificial Intelligence Laboratory, Vrije Universiteit  
1105 Brussel)
- 1106 Marcos, E. and Genovesio, A. (2016). Determining Monkey Free Choice Long before the Choice Is Made:  
1107 The Principal Role of Prefrontal Neurons Involved in Both Decision and Motor Processes. *Frontiers in*  
1108 *Neural Circuits* 10. doi:10.3389/fncir.2016.00075
- 1109 Marino, R. A., Trappenberg, T. P., Dorris, M., and Munoz, D. P. (2012). Spatial Interactions in the Superior  
1110 Colliculus Predict Saccade Behavior in a Neural Field Model. *Journal of Cognitive Neuroscience* 24,  
1111 315–336. doi:10.1162/jocn\_a\_00139
- 1112 McCarthy, M. M., Moore-Kochlacs, C., Gu, X., Boyden, E. S., Han, X., and Kopell, N. (2011). Striatal  
1113 origin of the pathologic beta oscillations in Parkinson's disease. *Proceedings of the National Academy*  
1114 *of Sciences* 108, 11620–11625. doi:10.1073/pnas.1107748108
- 1115 McIlwain, J. T. (1982). Lateral spread of neural excitation during microstimulation in intermediate gray  
1116 layer of cat's superior colliculus. *Journal of Neurophysiology* 47, 167–178
- 1117 McPeek, R. M. (2006). Incomplete Suppression of Distractor-Related Activity in the Frontal Eye Field  
1118 Results in Curved Saccades. *Journal of Neurophysiology* 96, 2699–2711. doi:10.1152/jn.00564.2006
- 1119 McPeek, R. M., Han, J. H., and Keller, E. L. (2003). Competition Between Saccade Goals in the Superior  
1120 Colliculus Produces Saccade Curvature. *Journal of Neurophysiology* 89, 2577–2590. doi:10.1152/jn.  
1121 00657.2002
- 1122 McPeek, R. M. and Keller, E. L. (2002). Saccade Target Selection in the Superior Colliculus During a  
1123 Visual Search Task. *Journal of Neurophysiology* 88, 2019–2034
- 1124 Meredith, M. A. and Ramoa, A. S. (1998). Intrinsic Circuitry of the Superior Colliculus: Pharmacophysio-  
1125 logical Identification of Horizontally Oriented Inhibitory Interneurons. *Journal of Neurophysiology* 79,  
1126 1597–1602
- 1127 Mink, J. W. (1996). The basal ganglia: focused selection and inhibition of competing motor programs.  
1128 *Progress in Neurobiology* 50, 381–425
- 1129 Mink, J. W. and Thach, W. T. (1993). Basal ganglia intrinsic circuits and their role in behavior. *Current*  
1130 *opinion in Neurobiology* 3, 950–957
- 1131 Mitchinson, B., Chan, T.-S., Chambers, J., Pearson, M., Humphries, M., Fox, C., et al. (2010). BRAHMS:  
1132 Novel middleware for integrated systems computation. *Advanced Engineering Informatics* 24, 49–61.  
1133 doi:10.1016/j.aei.2009.08.002
- 1134 Mitchinson, B. and James, S. S. (2015). BRAHMS. RRID: SCR\_015642

- 1135 Morn, J., Shibata, T., and Doya, K. (2013). The Mechanism of Saccade Motor Pattern Generation  
1136 Investigated by a Large-Scale Spiking Neuron Model of the Superior Colliculus. *PLoS ONE* 8, e57134.  
1137 doi:10.1371/journal.pone.0057134
- 1138 Munoz, D. P. (2002). Commentary: Saccadic eye movements: overview of neural circuitry. In *Progress in*  
1139 *Brain Research*, ed. D. M. J. Hyona, W. Heide and R. Radach (Elsevier), vol. Volume 140. 89–96
- 1140 Munoz, D. P. and Everling, S. (2004). Look away: the anti-saccade task and the voluntary control of eye  
1141 movement. *Nature Reviews Neuroscience* 5, 218–228. doi:10.1038/nrn1345
- 1142 Nambu, A., Yoshida, S.-i., and Jinnai, K. (1990). Discharge patterns of pallidal neurons with input from  
1143 various cortical areas during movement in the monkey. *Brain Research* 519, 183–191. doi:10.1016/  
1144 0006-8993(90)90076-N
- 1145 N'Guyen, S., Thurat, C., and Girard, B. (2014). Saccade learning with concurrent cortical and subcortical  
1146 basal ganglia loops. *Frontiers in Computational Neuroscience* 8. doi:10.3389/fncom.2014.00048
- 1147 Norman, D. A. and Shallice, T. (1986). Attention to action. In *Consciousness and self-regulation* (Springer).  
1148 1–18
- 1149 Nowotny, T. (2011). Flexible neuronal network simulation framework using code generation for NVidia  
1150 CUDA. *BMC Neuroscience* 12, P239. doi:10.1186/1471-2202-12-S1-P239
- 1151 Nowotny, T., Cope, A. J., Yavuz, E., Stimberg, M., Goodman, D. F., Marshall, J., et al. (2014). SpineML  
1152 and Brian 2.0 interfaces for using GPU enhanced Neuronal Networks (GeNN). *BMC Neuroscience* 15,  
1153 P148. doi:10.1186/1471-2202-15-S1-P148
- 1154 Olivier, E., Corvisier, J., Pauluis, Q., and Hardy, O. (2000). Evidence for glutamatergic tectotectal neurons  
1155 in the cat superior colliculus: a comparison with GABAergic tectotectal neurons. *European Journal of*  
1156 *Neuroscience* 12, 2354–2366
- 1157 Ottes, F. P., Van Gisbergen, J. A., and Eggermont, J. J. (1986). Visuomotor fields of the superior colliculus:  
1158 A quantitative model. *Vision Research* 26, 857–873. doi:10.1016/0042-6989(86)90144-6
- 1159 Papapavlou, C. and Moustakas, K. (2014). Physics-based modelling and animation of saccadic eye  
1160 movement
- 1161 Parent, A. and Hazrati, L. (1993). Anatomical aspects of information processing in primate basal ganglia.  
1162 *Trends in Neuroscience* 16, 111–116
- 1163 Quaia, C., Lefvre, P., and Optican, L. M. (1999). Model of the Control of Saccades by Superior Colliculus  
1164 and Cerebellum. *Journal of Neurophysiology* 82, 999
- 1165 Quaia, C., Par, M., Wurtz, R. H., and Optican, L. M. (2000). Extent of compensation for variations  
1166 in monkey saccadic eye movements. *Experimental Brain Research* 132, 39–51. doi:10.1007/  
1167 s002219900324
- 1168 Redgrave, P., Prescott, T. J., and Gurney, K. (1999). The basal ganglia: a vertebrate solution to the selection  
1169 problem? *Neuroscience* 89, 1009–1023
- 1170 Reppert, T. R., Lempert, K. M., Glimcher, P. W., and Shadmehr, R. (2015). Modulation of Saccade  
1171 Vigor during Value-Based Decision Making. *Journal of Neuroscience* 35, 15369–15378. doi:10.1523/  
1172 JNEUROSCI.2621-15.2015
- 1173 Richmond, P. (2015). DAMSON
- 1174 Richmond, P., Cope, A., Gurney, K., and Allerton, D. J. (2014). From Model Specification to Simulation  
1175 of Biologically Constrained Networks of Spiking Neurons. *Neuroinformatics* 12, 307–323. doi:10.1007/  
1176 s12021-013-9208-z
- 1177 Robinson, D. (1972). Eye movements evoked by collicular stimulation in the alert monkey. *Vision Research*  
1178 12, 1795–1808. doi:10.1016/0042-6989(72)90070-3

- 1179 Robinson, D. A. (1975). Oculomotor control signals. In *Basic mechanisms of ocular motility and their*  
1180 *clinical implications*, eds. G. Lennerstrand and P. Bach-y Rita (Oxford: Pergamon). 337–374
- 1181 Rovamo, J. and Virsu, V. (1979). An estimation and application of the human cortical magnification factor.  
1182 *Experimental Brain Research* 37, 495–510. doi:10.1007/BF00236819
- 1183 Schall, J. D. and Thompson, K. G. (1999). Neural selection and control of visually guided eye movements.  
1184 *Annual review of neuroscience* 22, 241–259
- 1185 Schiller, P. H., Sandell, J. H., and Maunsell, J. H. (1987). The effect of frontal eye field and superior  
1186 colliculus lesions on saccadic latencies in the rhesus monkey. *Journal of Neurophysiology* 57, 1033
- 1187 Schlag, J. D. (2002). Neurons that program what to do and in what order. *Neuron* 34, 177–178
- 1188 Schwartz, E. L. (1977). Spatial mapping in the primate sensory projection: Analytic structure and relevance  
1189 to perception. *Biological Cybernetics* 25, 181–194. doi:10.1007/BF01885636
- 1190 Schwartz, E. L. (1980). Computational anatomy and functional architecture of striate cortex: A spatial  
1191 mapping approach to perceptual coding. *Vision Res.* 20, 645–669
- 1192 Schweighofer, N., Arbib, M. A., and Dominey, P. F. (1996). A model of the cerebellum in adaptive control  
1193 of saccadic gain. *Biological Cybernetics* 75, 19–28
- 1194 Scudder, C. A. (1988). A new local feedback model of the saccadic burst generator. *J Neurophysiol* 59,  
1195 1454
- 1196 Seth, A., Sherman, M., Reinbolt, J. a., and Delp, S. L. (2011). OpenSim: a musculoskeletal modeling  
1197 and simulation framework for in silico investigations and exchange. *Procedia IUTAM* 2, 212–232.  
1198 doi:10.1016/j.piutam.2011.04.021
- 1199 Slotnick, S. D., Klein, S. A., Carney, T., and Sutter, E. E. (2001). Electrophysiological estimate of human  
1200 cortical magnification. *Clinical Neurophysiology* 112, 1349–1356
- 1201 Sparks, D. L. (2002). The brainstem control of saccadic eye movements. *Nature Reviews Neuroscience* 3,  
1202 952–964. doi:10.1038/nrn986
- 1203 Sparks, D. L. and Nelson, I. S. (1987). Sensory and motor maps in the mammalian superior colliculus.  
1204 *Trends in Neurosciences* 10, 312–317. doi:10.1016/0166-2236(87)90085-3
- 1205 Stanton, G. B., Goldberg, M. E., and Bruce, C. J. (1988a). Frontal eye field efferents in the macaque  
1206 monkey: I. Subcortical pathways and topography of striatal and thalamic terminal fields. *Journal of*  
1207 *Comparative Neurology* 271, 473–492. doi:10.1002/cne.902710402
- 1208 Stanton, G. B., Goldberg, M. E., and Bruce, C. J. (1988b). Frontal eye field efferents in the macaque  
1209 monkey: II. Topography of terminal fields in midbrain and pons. *The Journal of Comparative Neurology*  
1210 271, 493–506. doi:10.1002/cne.902710403
- 1211 Sterling, P. (1971). Receptive fields and synaptic organization of the superficial gray layer of the cat  
1212 superior colliculus. *Vision Research* 11, 309–IN47. doi:10.1016/0042-6989(71)90048-4
- 1213 Tabareau, N., Bennequin, D., Berthoz, A., Slotine, J.-J., and Girard, B. (2007). Geometry of the superior  
1214 colliculus mapping and efficient oculomotor computation. *Biological cybernetics* 97, 279–292
- 1215 Takagi, M., Zee, D. S., and Tamargo, R. J. (1998). Effects of Lesions of the Oculomotor Vermis on Eye  
1216 Movements in Primate: Saccades. *Journal of Neurophysiology* 80, 1911
- 1217 Talbot, S. and Marshall, W. (1941). Physiological Studies on Neural Mechanisms of Visual Localization  
1218 and Discrimination\*. *American Journal of Ophthalmology* 24, 1255–1264. doi:10.1016/S0002-9394(41)  
1219 91363-6
- 1220 Tehovnik, E. J., Sommer, M. A., Chou, I.-H., Slocum, W. M., and Schiller, P. H. (2000). Eye fields in the  
1221 frontal lobes of primates. *Brain Research Reviews* 32, 413–448. doi:10.1016/S0165-0173(99)00092-2
- 1222 Thelen, D. G. (2003). Adjustment of Muscle Mechanics Model Parameters to Simulate Dynamic  
1223 Contractions in Older Adults. *Journal of Biomechanical Engineering* 125, 70. doi:10.1115/1.1531112

- 1224 Thivierge, J.-P. and Marcus, G. F. (2007). The topographic brain: from neural connectivity to cognition.  
1225 *Trends in Neurosciences* 30, 251–259. doi:10.1016/j.tins.2007.04.004
- 1226 Thurat, C., NGuyen, S., and Girard, B. (2015). Biomimetic race model of the loop between the superior  
1227 colliculus and the basal ganglia: Subcortical selection of saccade targets. *Neural Networks* 67, 54–73.  
1228 doi:10.1016/j.neunet.2015.02.004
- 1229 Tipper, S. P., Howard, L. A., and Paul, M. A. (2001). Reaching affects saccade trajectories. *Experimental*  
1230 *Brain Research* 136, 241–249
- 1231 Van Gisbergen, J., Van Opstal, A., and Tax, A. (1987). Collicular ensemble coding of saccades based on  
1232 vector summation. *Neuroscience* 21, 541–555. doi:10.1016/0306-4522(87)90140-0
- 1233 Van Gisbergen, J. A. M., Van Opstal, A. J., and Schoenmakers, J. J. M. (1985). Experimental test of two  
1234 models for the generation of oblique saccades. *Experimental brain research* 57, 321–336
- 1235 van Opstal, A. J. and Goossens, H. H. L. M. (2008). Linear ensemble-coding in midbrain superior colliculus  
1236 specifies the saccade kinematics. *Biological Cybernetics* 98, 561–577. doi:10.1007/s00422-008-0219-z
- 1237 Van Opstal, A. J., Hepp, K., Hess, B. J., Straumann, D., and Henn, V. (1991). Two-rather than three-  
1238 dimensional representation of saccades in monkey superior colliculus. *Science* 252, 1313–1315
- 1239 Vokoun, C. R., Huang, X., Jackson, M. B., and Basso, M. A. (2014). Response Normalization in the  
1240 Superficial Layers of the Superior Colliculus as a Possible Mechanism for Saccadic Averaging. *Journal*  
1241 *of Neuroscience* 34, 7976–7987. doi:10.1523/JNEUROSCI.3022-13.2014
- 1242 Vokoun, C. R., Jackson, M. B., and Basso, M. A. (2010). Intralaminar and Interlaminar Activity within the  
1243 Rodent Superior Colliculus Visualized with Voltage Imaging. *Journal of Neuroscience* 30, 10667–10682.  
1244 doi:10.1523/JNEUROSCI.1387-10.2010
- 1245 Vokoun, C. R., Jackson, M. B., and Basso, M. A. (2011). Circuit dynamics of the superior colliculus  
1246 revealed by in vitro voltage imaging: Vokoun et al. *Annals of the New York Academy of Sciences* 1233,  
1247 41–47. doi:10.1111/j.1749-6632.2011.06166.x
- 1248 Waitzman, D. M., Ma, T. P., Optican, L. M., and Wurtz, R. H. (1991). Superior colliculus neurons mediate  
1249 the dynamic characteristics of saccades. *Journal of Neurophysiology* 66, 1716–1737
- 1250 Walker, R., Deubel, H., Schneider, W. X., and Findlay, J. M. (1997). Effect of remote distractors on saccade  
1251 programming: evidence for an extended fixation zone. *Journal of neurophysiology* 78, 1108–1119
- 1252 Wickens, J. (1997). Basal ganglia: structure and computations. *Network: Computation in Neural Systems*  
1253 8, 77–109
- 1254 Wilson, C. and Kawaguchi, Y. (1996). The origins of the two-state spontaneous membrane potential  
1255 fluctuations of neostriatal spiny neurons. *The Journal of Neuroscience* 16, 2397–2410
- 1256 Wilson, C. J. (2004). A Model of Reverse Spike Frequency Adaptation and Repetitive Firing of Subthalamic  
1257 Nucleus Neurons. *Journal of Neurophysiology* 91, 1963–1980. doi:10.1152/jn.00924.2003
- 1258 Wu, H. H., Williams, C. V., and McLoon, S. C. (1994). Involvement of nitric oxide in the elimination  
1259 of a transient retinotectal projection in development. *SCIENCE-NEW YORK THEN WASHINGTON-*,  
1260 1593–1593
- 1261 Wurtz, R. H. and Goldberg, M. E. (1972). Activity of superior colliculus in behaving monkey. III. Cells  
1262 discharging before eye movements. *J Neurophysiol* 35, 575–586

## FIGURES

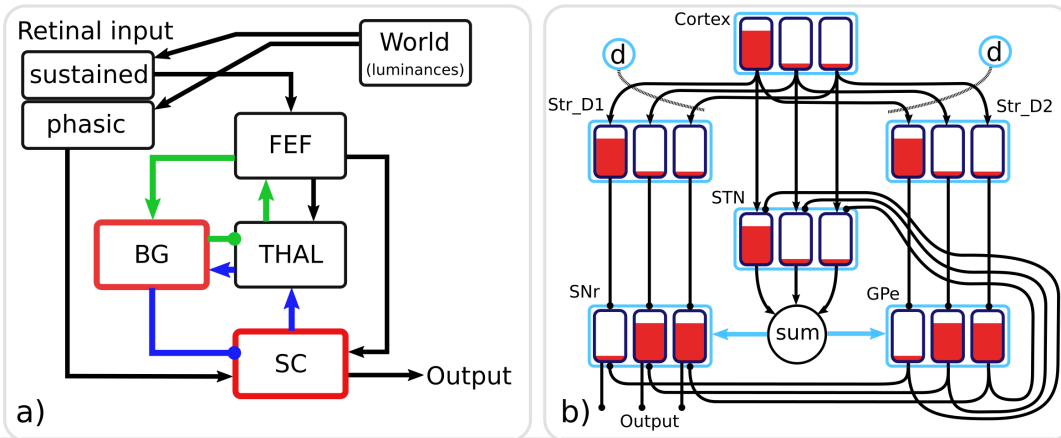


**Figure 6. a) The macroscopic architecture of the Cope-Chambers-Prescott-Gurney model.** The main nuclei modelled as brain systems are: basal ganglia (BG), frontal eye fields (FEF), thalamus (THAL) and superior colliculus (SC). The retinal input is presented via non-biologically plausible retinal populations. The loops through basal ganglia, which define the architecture, are shown with coloured lines: the cortical loop (through FEF and THAL) in green and the sub-cortical loop (through SC and THAL) in blue. Connections with arrowheads indicate excitatory connections, those with circles are inhibitory. A red border indicates that the box represents a sub-system of two or more populations; a black box indicates (at least, within the context of the model) a single neural population. The BG box is expanded in: **b) The basal ganglia model component.** This shows a basal ganglia comprising striatum (Str\_D1 & Str\_D2), subthalamic nucleus (STN), globus pallidum externum (GPe) and substantia nigra reticulata (SNr). The model has three action channels shown as black boxes within each blue population border. Three channels of cortical input to the BG are also depicted. Red indicates the activation level of a given channel, helping to illustrate the selection mechanism. For example, the channel indicated by the leftmost bar has a high salience (cortical input) and excites activity in Str\_D1 which then inhibits the leftmost bar in SNr. The diffuse projection from STN is equivalent to summing its projections channel-wise, and then projecting the sum to all channels of its target populations (the blue arrows indicate that all channels of GPe and SNr are targeted by the connection). Dopaminergic modulation of the inputs to the striatum are indicated by the blue circles labelled 'd' and the dotted lines. The SNr sends inhibitory output projections to its targets.

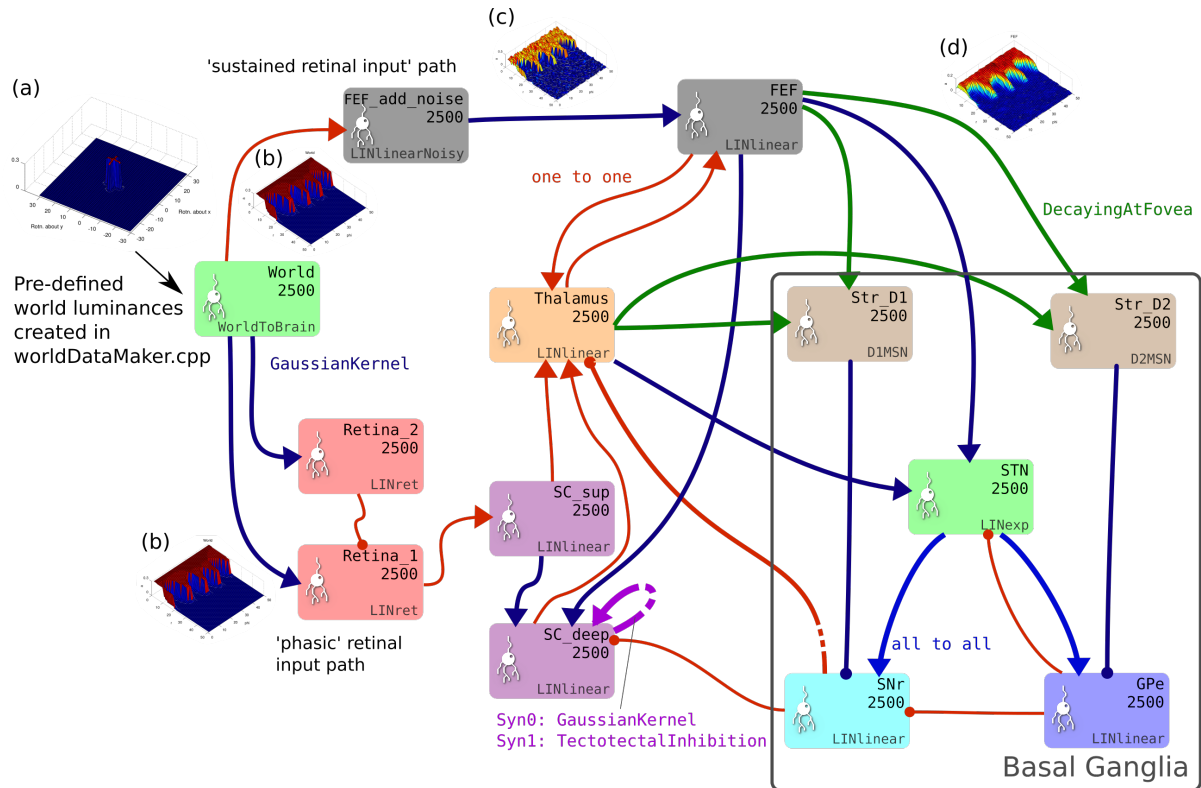


**Figure 7.** The brain model. This is the SpineCreator ‘network layer’ view of the model. Each box represents a neural population with 2500 elements, arranged in a  $50 \times 50$  grid. The SpineML component name is printed on the bottom right corner of each population box and the population name is at the top. The overall connectivity between populations is represented by the projection arrows with the colour indicating the connectivity scheme (one-to-one connections are red, Gaussian kernel connections are dark blue and so on). Excitatory connections have arrowheads and inhibitory connections have circles, although for details of the behaviour of the connections, the weight-update and post-synapse components must be studied. Briefly, the model comprises a *World* population, into which a retinotopically organised view of the world is introduced. This information is passed into cortical populations (FEF) and subcortical populations (SC) via a simple model of the retina. These feed a cortico-thalamo-basal ganglia loop, which selects which region of the deep layer of superior colliculus should be disinhibited, allowing activity to build up therein. The five populations comprising the basal ganglia are enclosed in a grey outline. Note that substantia nigra pars compacta is not modelled here, instead the level of dopamine in the striatum is set via a parameter in the Str\_D1 and Str\_D2 populations

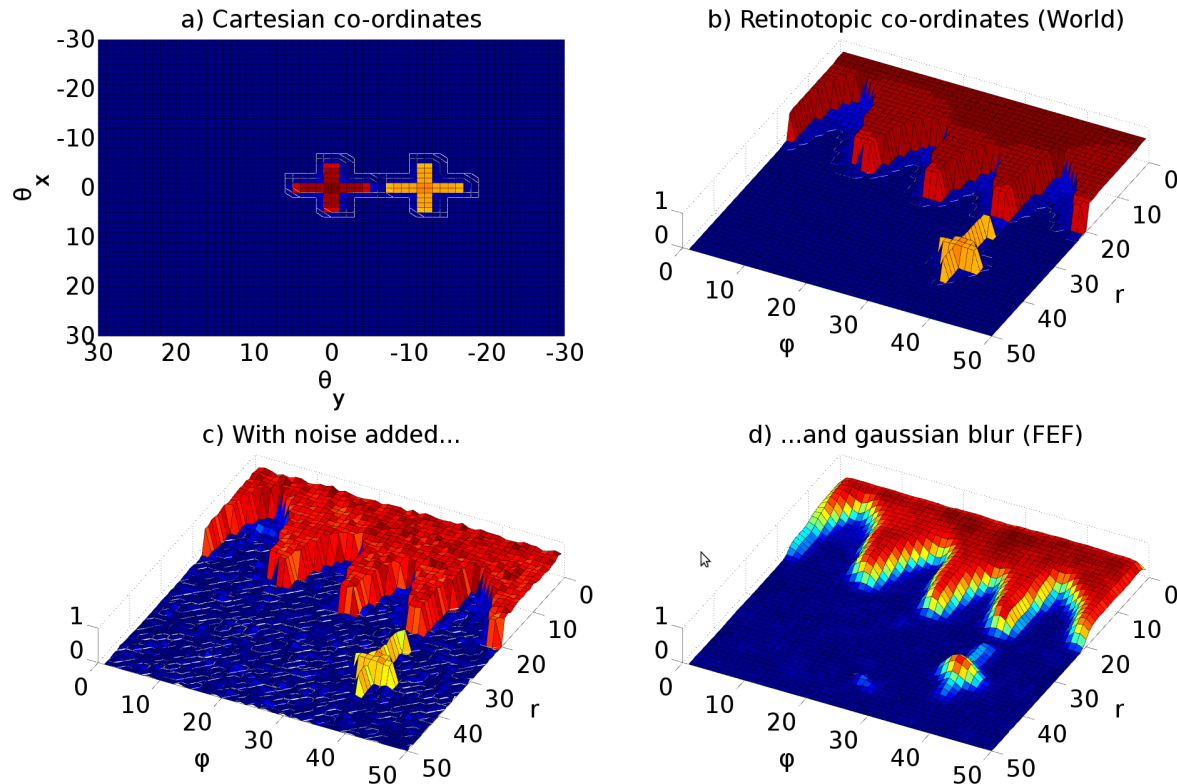


**Figure 8.** Representative mapping from eye's frame of reference in Cartesian co-ordinates to retinotopic co-ordinates. (a) The mapping of luminances in the eye's frame of reference. The world input is pre-defined by a JSON configuration file. Luminance position, size and shape can be defined in this file, along with the times at which luminances appear and disappear. The worldDataMaker.cpp code computes the locations of the luminances in the eye's frame of reference, given its rotational state. It also computes a 2D Gaussian convolution of the luminances. Here, there are two cross shaped luminances spanning  $10^\circ$ , one of value 0.8 at the fixation point (0,0) and one of value 0.5 at a peripheral position (0,- $12^\circ$ ). Note that these crosses have the same 'bar width' of  $2^\circ$  as the crosses used in the simulations, but their span of  $10^\circ$  is greater than the  $6^\circ$  used in the simulations, to make these images clearer. (b) The locations of the luminances in the eye's frame of reference are then converted into retinotopic co-ordinates, with centrally located luminances being represented at low values of  $r$  and more peripheral luminances having higher values of  $r$ .  $\phi$  encodes rotational angle: 1 and 50 encode upward movement; 13 is left; 25 is down; 37 is right. The output of the World component is fed into FEF\_add\_noise and into the retinal neuron populations. The colour map makes it possible to distinguish between the two crosses. (c) The FEF\_add\_noise populations adds a level of noise to the signal representing processing of the signal in visual cortex. (d) A Gaussian projection from FEF\_add\_noise to FEF further blurs the activity in FEF. FEF is the input to the basal ganglia and one input to superior colliculus.

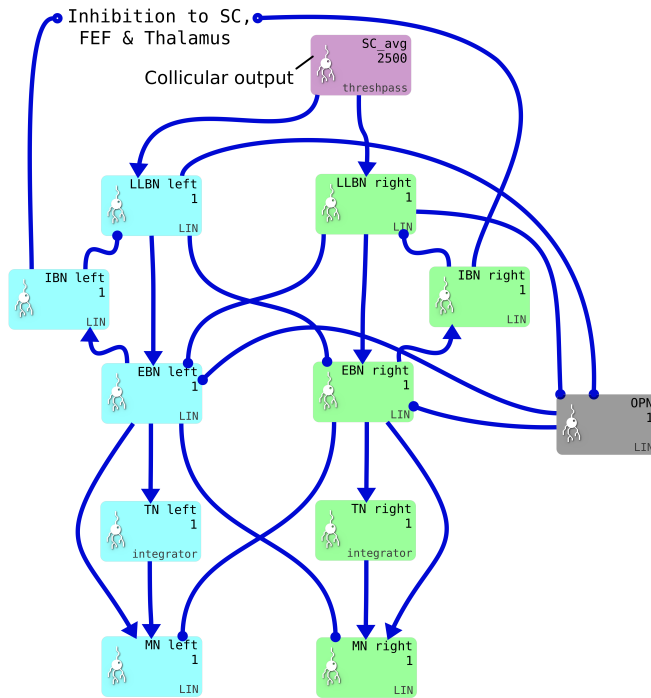


**Figure 9.** One pair of channels of the saccadic burst generator (SBG) for left (cyan) or right (green) movements. Collicular activity in SC\_avg excites the channels via SBG weight maps. Each box represents a neural population and shows the population name, the number of neural elements (here 2500 or 1) and the SpineML component name; LIN for Leaky integrator or *integrator*. Key: LLBN: Long lead burst neurons; IBN: Inhibitory burst neurons; OPN: Omnipause neurons; EBN: Excitatory burst neurons; TN: Tonic neurons; MN: Motoneurons.

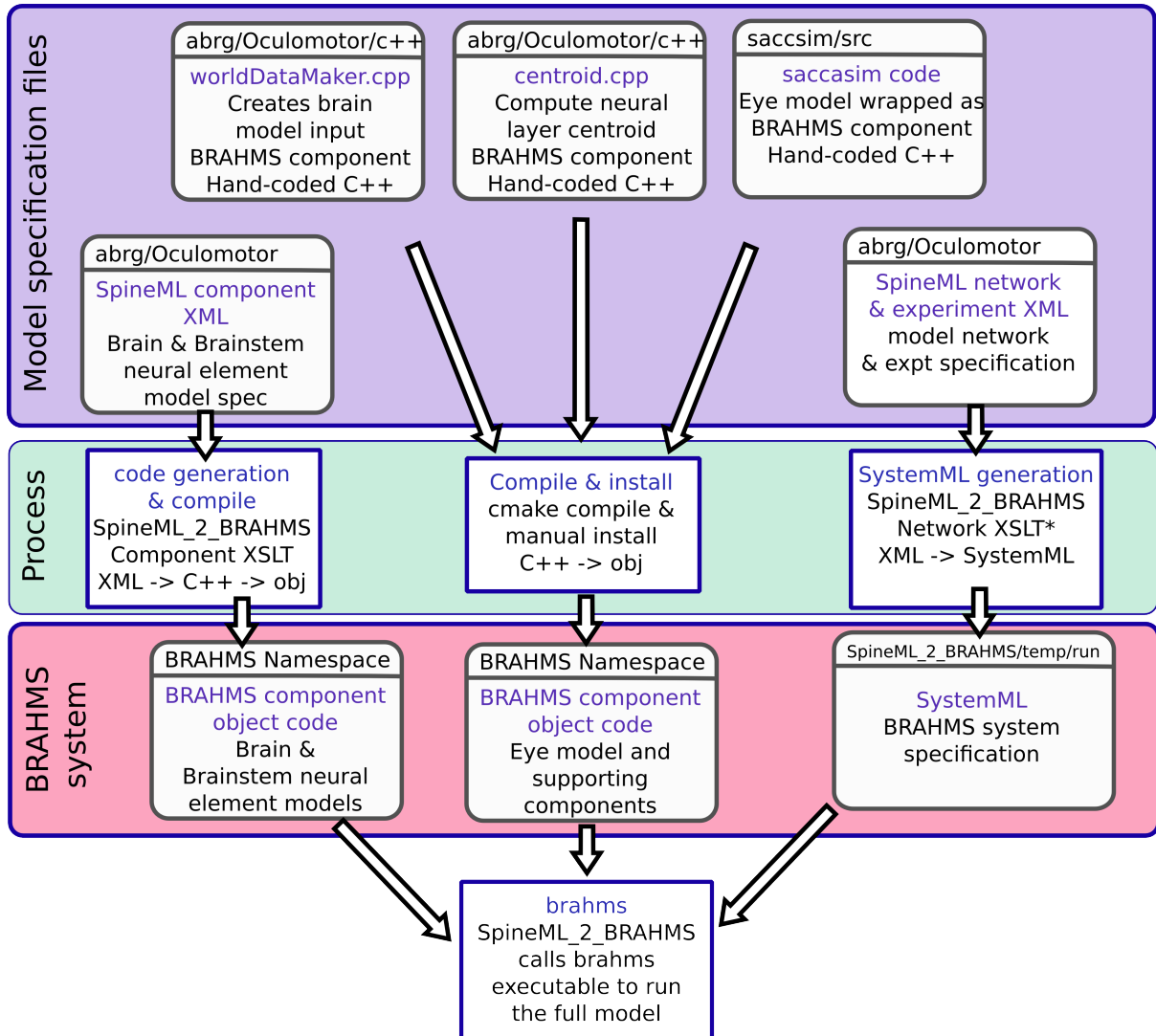


**Figure 10.** The model framework. The model is specified using a combination of declarative XML files and hand-coded C++. These original model specifications are shown within the blue box. b) The green box shows the processes which are applied to the model specification to produce the BRAHMS system. Most of the process is defined within the scripts which make up SpineML\_2\_BRAHMS, but the hand-written components must be manually compiled and installed within the BRAHMS Namespace, allowing the BRAHMS executable to locate them at runtime. c) The red box shows the resulting BRAHMS system ready to be executed by the BRAHMS executable. In practice, this call is made by SpineML\_2\_BRAHMS.

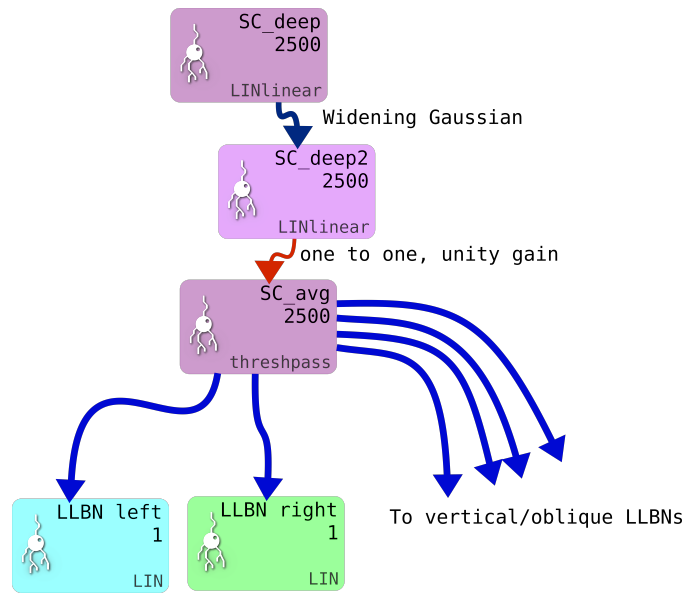


**Figure 11.** Showing the additional deep layer of superior colliculus (SC\_deep2) and the output layer (SC\_avg, named for the fact that in an earlier version of the model, it received the output of the centroid of SC\_deep). The widening Gaussian projection is shown as the arrow between SC\_deep and SC\_deep2.

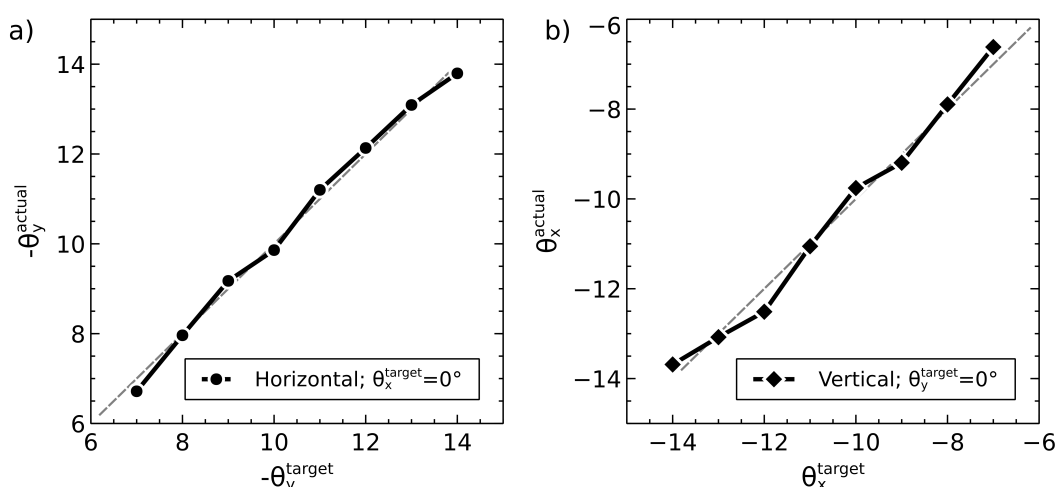


**Figure 12.** Accuracy at different target eccentricities for fixation luminance 0.2 and target luminance 0.3.

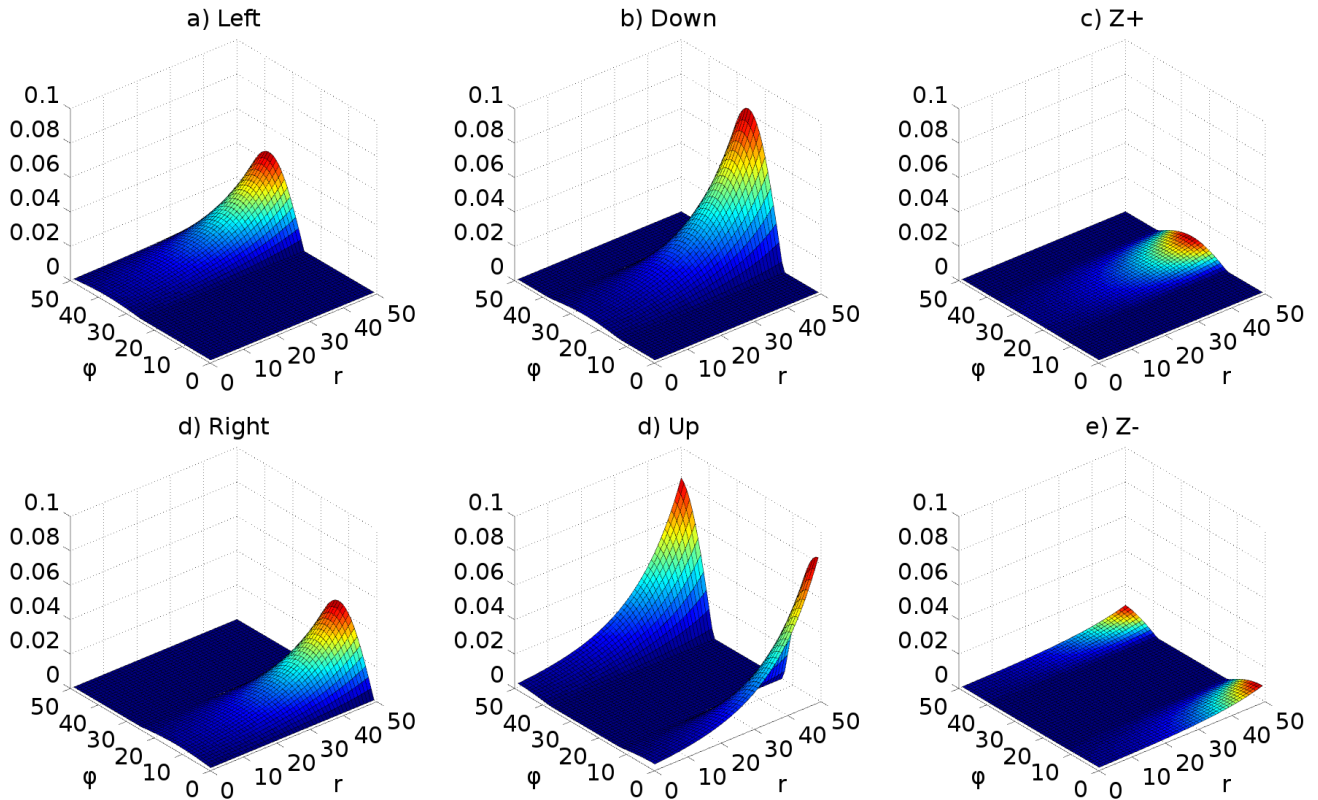


**Figure 13.** Weight maps for the connections between the output layer of superior colliculus and the six long lead burst neurons of the saccadic burst generator model. Each map increases exponentially with increasing  $r$ , multiplied by  $\cos(\phi)$  about its ‘active’ axis.

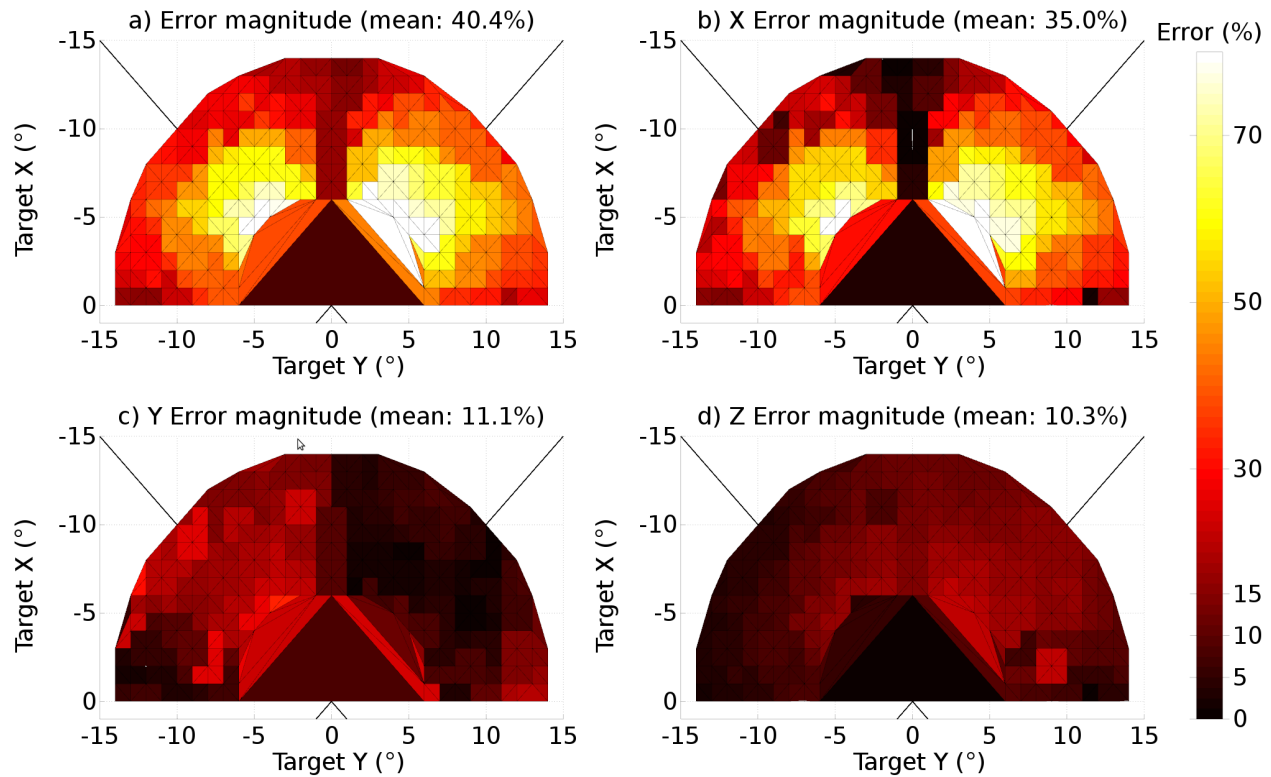


**Figure 14.** The end-point error surface for the original, naïve model (TModel3). a) The ratio of the magnitudes of the total error vector and the target vector, expressed as a percentage. b) The ratio of the magnitude of the  $x$  component of the error vector to the magnitude of the target vector, expressed as a percentage. c) As (b) but for the  $y$  component. d) As (b), for  $z$  component. All colour maps are shown with the same scale. The target rotations,  $\theta_x^t$  and  $\theta_y^t$  are denoted ‘Target X’ and ‘Target Y’ in the figure.

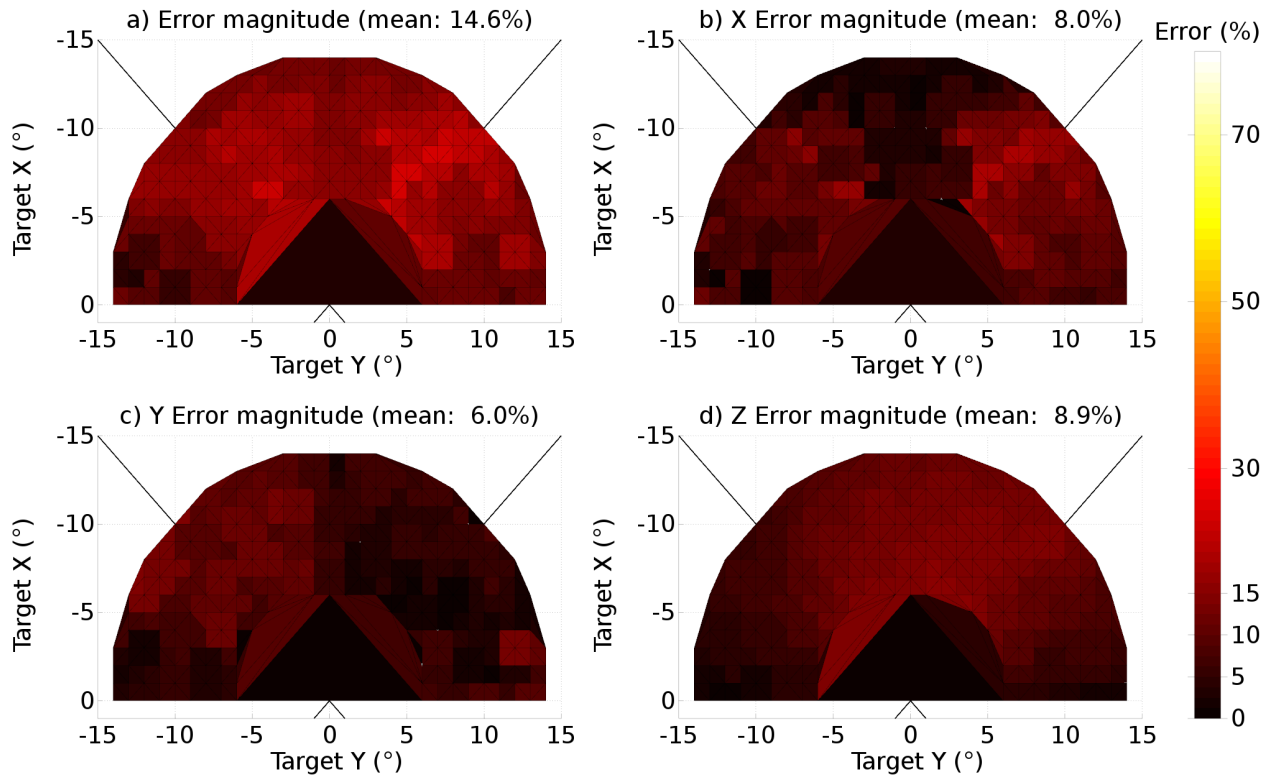


**Figure 15.** The end-point error surface for the model in which a widening projection field was added to the model of the superior colliculus. a) The ratio of the magnitudes of the total error vector and the target vector, expressed as a percentage. b) The ratio of the magnitude of the  $x$  component of the error vector to the magnitude of the target vector, expressed as a percentage. c) As (b) but for the  $y$  component. d) As (b), for  $z$  component. All colour maps are shown with the same scale. The target rotations,  $\theta_x^t$  and  $\theta_y^t$  are denoted ‘Target X’ and ‘Target Y’ in the figure. Note that the range of the colour scale is 0 to 20%, a much smaller range than the range in Fig 14.

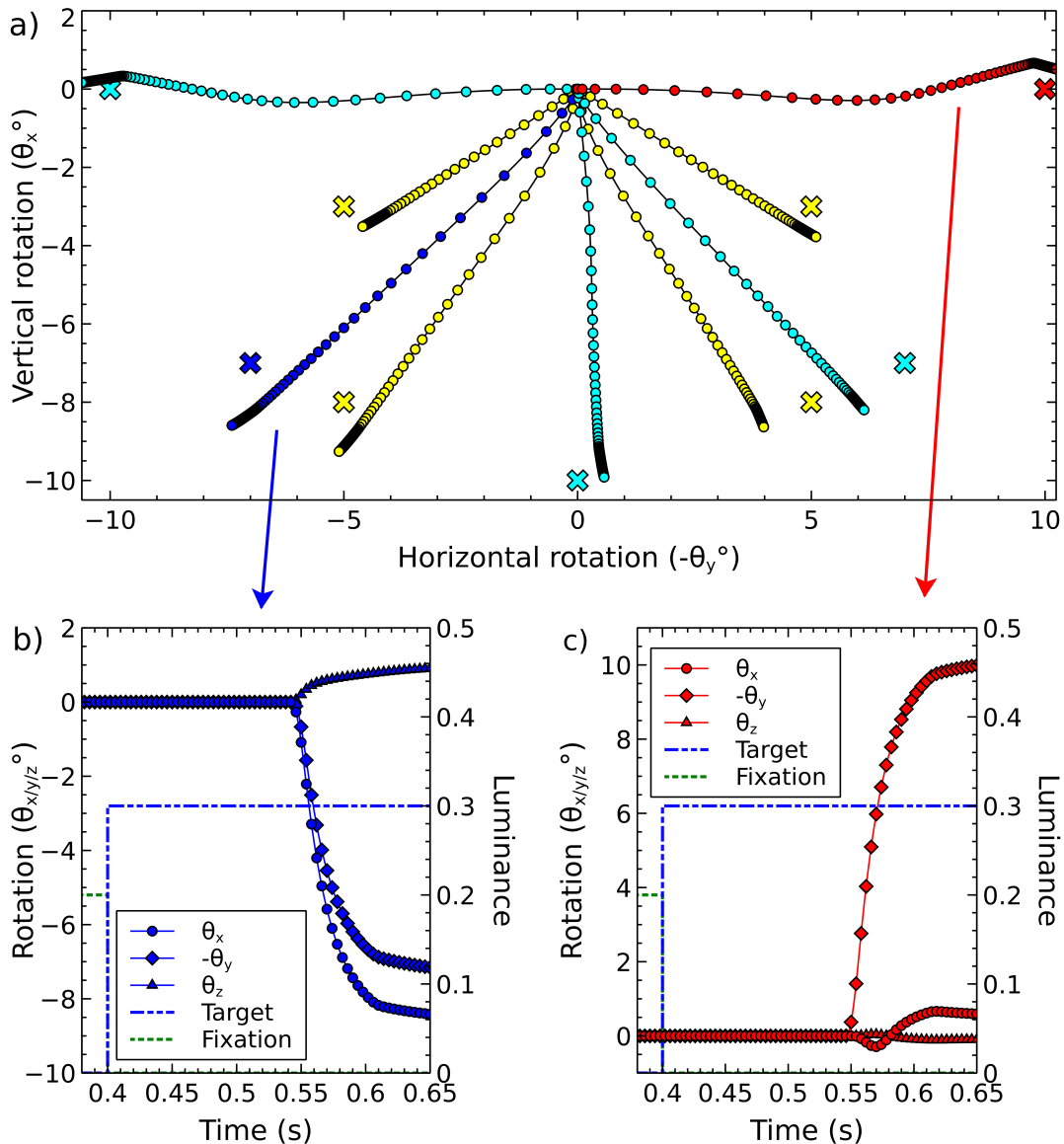


**Figure 16.** Representative single saccades. a) Trajectories from 9 saccades to a single target at 9 different locations. In each case, a fixation cross luminance of magnitude 0.2 was displayed at (0,0), the start position of the eye, until time 0.4 s. The target luminance, magnitude 0.3 was illuminated at time 0.4 s. Trajectory shape is dependent on the target position, and there is a variable amount of error in the end-points achieved by the model. Colour is used in this diagram as an aid to distinguishing different saccades and their targets; for a given saccade, the target location is given by the cross of the same colour closest to the end of the trajectory. b) The three rotational components of the ‘blue’ saccade, to target location (-7,-7). c) The three rotational components of the ‘red’ saccade, to target location (0,-10).

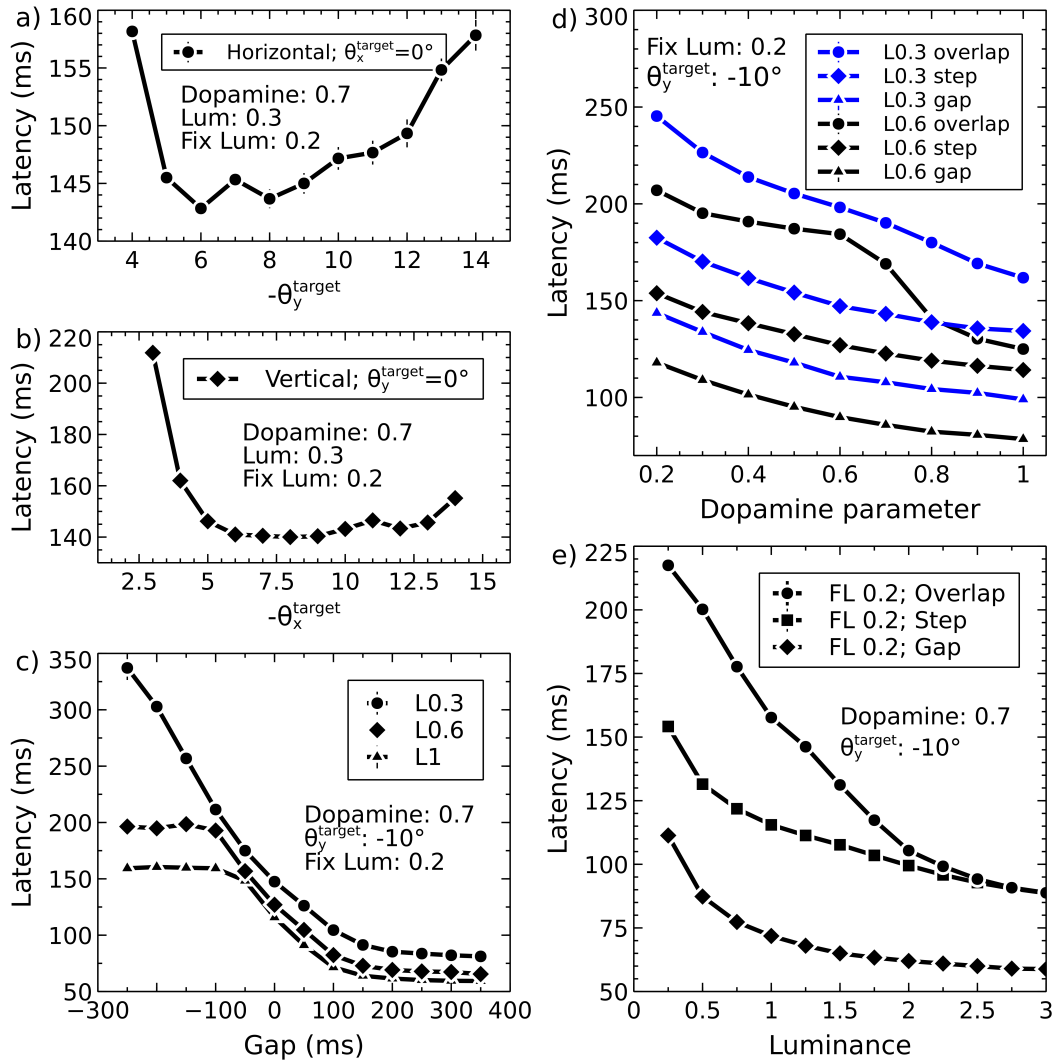


**Figure 17.** Exploring saccade latencies. a) Latency to first movement as a function of target eccentricity for horizontal targets. b) Latency vs. eccentricity for vertical targets. c) Latency vs. gap at three different luminance values. d) The effect of the dopamine parameter on saccade latencies in gap, step and overlap conditions, for two different target luminances. e) Saccade vs. luminance showing gradual transition between reflexive and express behaviour.

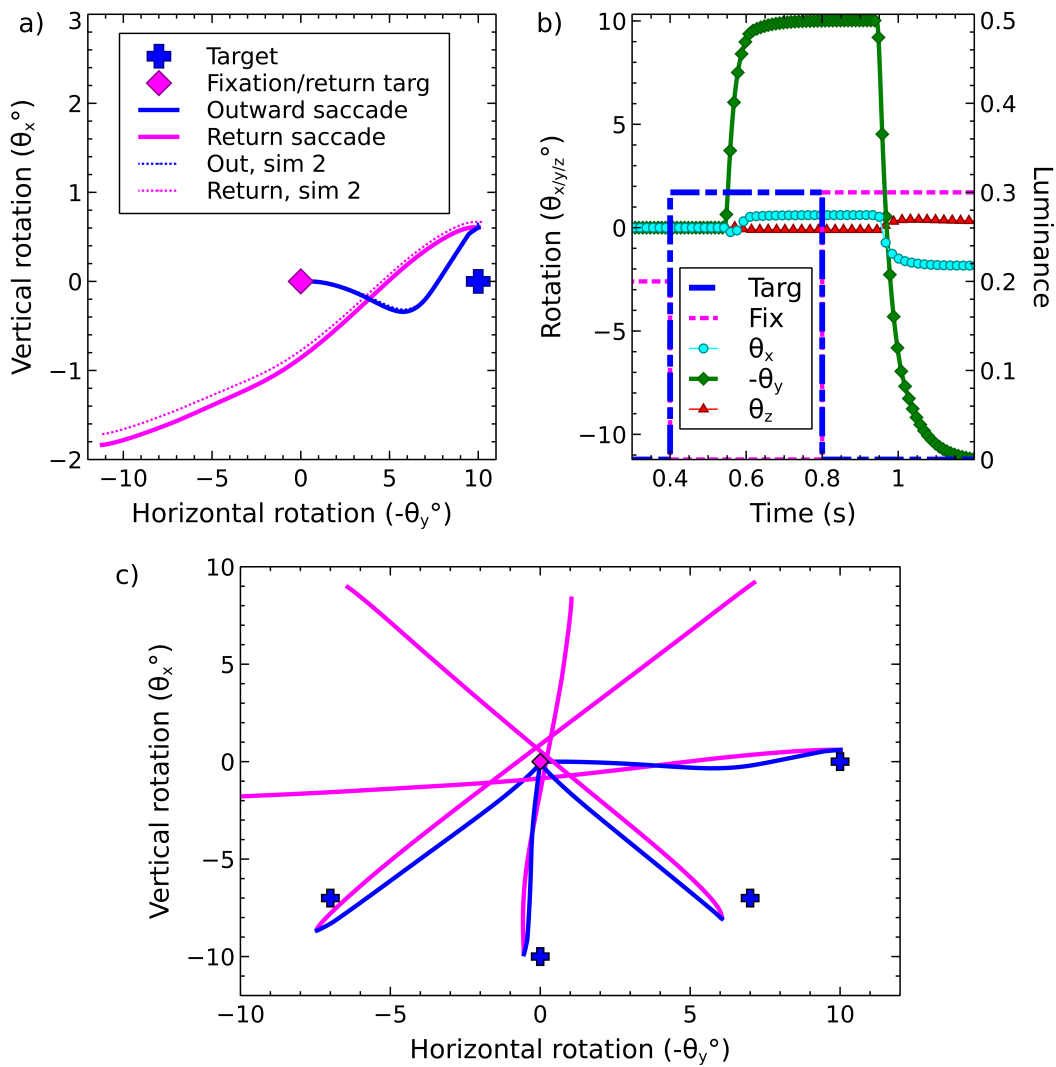


**Figure 18.** There and back - a saccade to a target, followed by return to the original fixation. a) Out and return saccade to a target at  $(0, -10^\circ)$  b) Rotational components of the saccade shown in (a). c) Outward and return trajectories for the saccade shown in (a) alongside saccades to three other targets.

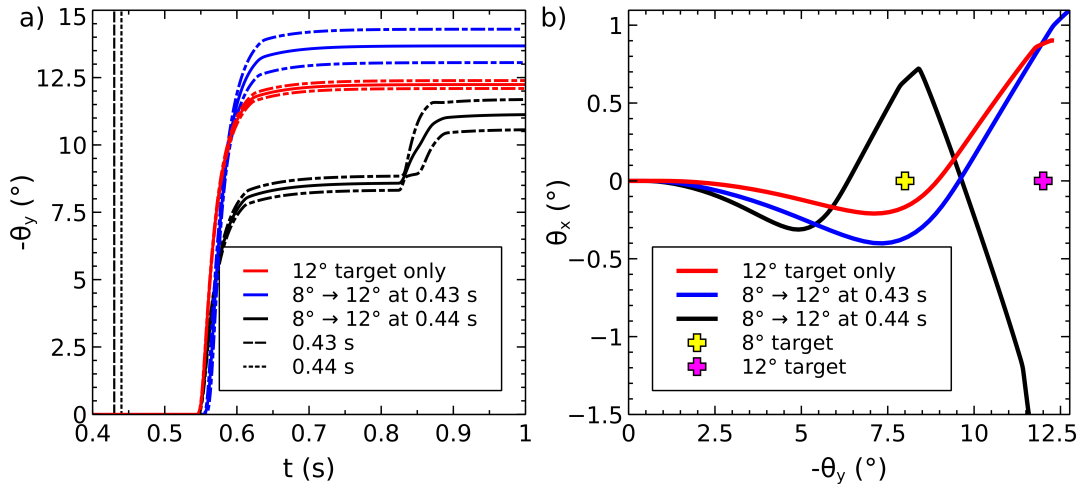


**Figure 19.** Double steps. The effect of illuminating a first target at  $8^\circ$  or  $12^\circ$ , followed by a second target at  $12^\circ$  or  $8^\circ$ . a) Horizontal rotation of the eye plotted vs. time for a saccade to the  $12^\circ$  target only (red), and to an  $8^\circ$  target at 0.4 s followed by a  $12^\circ$  target after 30 ms (blue) or 40 ms (black). The timings are indicated by vertical lines. When the second target is presented up to 30 ms after the initial target, the initial target has not had time to dominate the output saccade and a saccade to a location close to the second target is made. If the delay is 40 ms or more, the activity from the initial target has time to cause a built up of activity in SC\_deep and an initial saccade close to the first target is made, followed, after a longer than usual latency period, with a second saccade closer to the second target. In this graph, the mean of five separate simulations is plotted along with  $\pm 1$  standard deviation around the mean. b) The  $\theta_x/\theta_y$  trajectories corresponding to the data presented in (a).